AD_____

Award Number: DAMD17-02-1-0171

TITLE: Role of Oligomeric α-Synuclein in Mitochondrial Membrane Permeabilization and Neurodegeneration in Parkinson's Disease

PRINCIPAL INVESTIGATOR: Seung-Jae Lee, Ph.D.

CONTRACTING ORGANIZATION: The Parkinson's Institute
Sunnyvale, California 94089-1605

REPORT DATE: August 2004

TYPE OF REPORT: Final

PREPARED FOR: U.S. Army Medical Research and Materiel Command
Fort Detrick, Maryland 21702-5012

REPORT DOCUMENTATION PAGE

Form Approved
OMB No. 074-0188

1. AGENCY USE ONLY (Leave blank)	2. REPORT DATE	3. REPORT TYPE AND DATES COVERED
	August 2004	Final (19 Nov 01 - 30 Jul 04)

4. TITLE AND SUBTITLE
Role of Oligomeric α-Synuclein in Mitochondrial Membrane Permeabilization and Neurodegeneration in Parkinson's Disease

5. FUNDING NUMBERS
DAMD17-02-1-0171

6. AUTHOR(S)
Seung-Jae Lee, Ph.D.

7. PERFORMING ORGANIZATION NAME(S) AND ADDRESS(ES)
The Parkinson's Institute
Sunnyvale, California 94089-1605

E-Mail: Slee@thepi.org

8. PERFORMING ORGANIZATION REPORT NUMBER

9. SPONSORING / MONITORING AGENCY NAME(S) AND ADDRESS(ES)
U.S. Army Medical Research and Materiel Command
Fort Detrick, Maryland 21702-5012

11. SUPPLEMENTARY NOTES
Original contains color plates. All DTIC reproductions will be in black and white.

12a. DISTRIBUTION / AVAILABILITY STATEMENT
Approved for Public Release; Distribution Unlimited

12b. DISTRIBUTION CODE

13. ABSTRACT (Maximum 200 Words)

A growing body of evidence suggests that aggregation of α-synuclein might be the fundamental cause of many neurodegenerative diseases. Several groups have developed cell culture models to study the cytotoxic effect of α-synuclein, and some of them indeed have observed enhanced cell death when α-synuclein, especially its mutant forms, was overexpressed. However, the link between α-synuclein aggregation and cell death has not been clearly addressed in these model systems, nor are the molecular mechanisms underlying the toxicity known. From the studies of the current project, we have demonstrated that the formation of prefibrillar oligomeric α-synuclein aggregates is tightly associated with Golgi fragmentation and cell death in both neuronal and non-neuronal cell models, suggesting the prefibrillar intermediates as being pathogenic species. On the other hand, fibrillar inclusion bodies seem to be a consequence of cellular effort to remove toxic protein aggregates and damaged organelles from cytoplasm. Finally, we show that α-synuclein aggregation causes the disruption of the microtubule network and the intracellular trafficking, leading to Golgi fragmentation and neuritic degeneration. These data identify microtubule dysfunction as being the link between α-synuclein aggregation and neurodegeneration.

14. SUBJECT TERMS
Parkinson's disease, synuclein, amyloid fibril, protein aggregation, Golgi apparatus, inclusion body, microtubule, neurodegeneration

15. NUMBER OF PAGES
37

16. PRICE CODE

17. SECURITY CLASSIFICATION OF REPORT	18. SECURITY CLASSIFICATION OF THIS PAGE	19. SECURITY CLASSIFICATION OF ABSTRACT	20. LIMITATION OF ABSTRACT
Unclassified	Unclassified	Unclassified	Unlimited

Table of Contents

A. Introduction

Many human neurological disorders, including Parkinson's disease (PD), dementia with Lewy bodies, and multiple system atrophy, are characterized by amyloid-like fibrillar aggregates of α-synuclein (α-syn), such as Lewy bodies (LBs) and Lewy neurites (Hardy and Gwinn-Hardy, 1998; Trojanowski et al., 1998). While the direct role of fibrils and inclusion bodies in disease progression is the subject of intense debate, recent *in vitro* studies revealed various non-fibrillar species during the course of fibrillation and suggested a possibility that these metastable intermediate species, not the fibrils themselves, might elicit cytotoxicity (Conway et al., 2000; Conway et al., 2001). Elucidating which particular aggregate species possess the principal cytotoxic effect holds the key to understanding the etiologic role of protein aggregation in the disease pathogenesis. Study of this problem, however, has been hampered by the lack of experimental system in which intermediates of the endogenous fibrillation process can be biochemically defined and analyzed. We have recently established such an experimental cell system, and the goal of the current study is to elucidate the mechanisms of α-syn fibrillation and assess the effects of prefibrillar intermediates in the cytoplasm.

B. Body

B.1. Mechanisms of α-syn fibrillation and inclusion formation in cells

In order to understand the mechanism of α-syn aggregation in cells, the first objective of our study was to characterize the structural and compositional properties of different aggregate species. Specifically, we have addressed following questions. (i) What is the end product of α-syn aggregation process in cells? (i.e., is it the fibril or other aggregate form?) (ii) What are the intermediates of α-syn fibrillation in cells? (iii) Is the fibrillation process linked to the inclusion formation process and if so, how? In this study, using a combination of biochemical fractionation, immunofluorescence labeling, and electron microscopy (EM), we have accomplished following. For details, see appendix (A) 1, Lee and Lee. Figures that are referenced in this section can be found in A1.

1. ***Isolation of different aggregate species from the cytoplasm.*** Overexpression of α-syn in cells spontaneously produce two types of aggregates that are distinct in their sizes and cytoplasmic distributions. One type is represented by small punctate aggregates that are dispersed throughout the cytoplasm, and the other is large juxtanuclear inclusion bodies (Fig 1). In order to further characterize different types of α-syn aggregates, these aggregates were separated using a series of extractions and differential and density-gradient centrifugations (for details, see Fig. 2A and materials and methods in appendix 1). Western blot analysis of the fractions (frs) has identified three distinct fractions containing SDS-resistant α-syn aggregates (fr 2, fr 4, and 80 g pellet) (Fig. 2B), confirming the presence of different aggregate species.

2. ***Structural properties of cytoplasmic aggregates.*** The juxtanuclear inclusion bodies bind to thioflavin S (Fig. 1B and 3), a fluorescent dye specific for the highly ordered cross β-sheet structure, thus an indicative of the amyloid-like fibrillar structures. In contrast, the small punctate aggregates (both the frs 2 and 4) are thioflavin S-negative (Fig. 1A and 3), indicating a non-fibrillar conformation. The difference in the dye binding properties

suggests that these two types of aggregates have different structural properties. To further analyze the ultrastructural features of α-syn aggregates, the fractions were examined by immuno-EM. The aggregates in both the fr 2 and fr 4 appear to be non-fibrillar spheres (Fig. 4A and B). Random measurement of the diameter of these spheres shows the different size distributions, and the calculated mean diameters for fr 2 and fr 4 were 24 nm and 34 nm, respectively. On the other hand, EM analysis showed that the 80 g pellet contained the large inclusion bodies that are filled with fibril structures (Fig. 5A and B). The fibrils isolated from the inclusions are 8-13 nm in width and are clearly labeled with α-syn antibody (Fig. 5B). These fibrils resemble the ones isolated from human LBs (Spillantini et al., 1998) or the inclusions of the transgenic mice (Giasson et al., 2002). Thicker structures, which appear to be fibril bundles, are also frequently observed (Fig. 5C). These ultrastructural morphologies, along with the thioflavin S binding property, demonstrate that α-syn aggregation process in our cell model produces the inclusion bodies that are composed of α-syn fibrils, thus suggesting that this process of inclusion body formation in these cells may resemble the process of LB formation in human brain.

3. ***Compositional properties of cytoplasmic aggregates.*** To determine whether the inclusion bodies in our cell system share the protein components with human LBs, we co-stained the cells for α-syn with ubiquitin, α-subunit of 20S proteasome, or hsp70 (Ii et al., 1997; Spillantini et al., 1998; Auluck et al., 2002). Like human LBs, large juxtanuclear inclusion bodies were positive for all these proteins (Fig. 1 B). On the other hand, most of peripheral punctate aggregates were not stained with ubiquitin, the proteasome subunit, or hsp70 (Fig. 1A). Consistent with these findings, immunofluorescence staining of the fractionated aggregates showed that the small aggregates did not contain ubiquitin, hsp70, or 20S proteasome α-subunit, whereas the large inclusion bodies in the 80 g pellet were positive for these proteins (Fig. 3B, C, and D). These results confirm that the cells produce different types of α-syn aggregates with distinct conformational and compositional properties and that the separation of these aggregates can be achieved using our fractionation procedure.

4. ***Protofibril-to-fibril transition in the cytoplasm is linked to the microtubule-dependent inclusion-forming process.*** Time course analysis of the aggregates showed that the fr 2 aggregates appeared first, followed by the fr 4 aggregates and subsequently by the fibrillar inclusion bodies (Fig. 6). The fact that these aggregates appear sequentially suggests precursor-product relationship between them. It has been demonstrated with a number of proteins that the juxtanuclear inclusion formation requires the microtubule-dependent transport of peripheral small aggregates to the pericentriolar region (Johnston et al., 1998; Garcia-Mata et al., 1999). To test if microtubule-dependent transport is important for the formation of α-syn inclusion body, we treated the cells with a microtubule-disrupting agent, nocodazole, and assessed the inclusion formation in two ways. First, the number of inclusion bodies was counted after the immunofluorescence staining (Fig. 7A). Second, the relative amounts of inclusion bodies and small non-fibrillar aggregates were measured after the fractionation (Fig. 7B). Both analyses clearly show the decrease of the inclusion bodies after nocodazole treatment, implicating the importance of microtubule-dependent transport system in the inclusion formation. Furthermore, the fractionation experiment shows that the reduction of inclusion bodies is

accompanied by the increase of the small aggregates (Fig. 7B), confirming that the small spherical aggregates are the precursors for the fibrillar inclusions. Interestingly, when the microtubule is disrupted, bigger foci were frequently found in the periphery of the cell (Fig. 7C), which implies that the peripheral aggregates can grow bigger to a certain extent, if their transport to the pericentriolar region is blocked. This finding raised a question as to whether the large foci that are grown in the periphery of the cell can acquire the characteristics of the juxtanuclear inclusion bodies. To address this question, we have investigated the thioflavin S binding property and the immunoreactivities for the proteins that are found in the inclusion bodies. Unlike the juxtanuclear inclusion bodies, the large peripheral foci are thioflavin S-negative, indicating non-fibrillar nature of the aggregates, and devoid of ubiquitin, hsp70, and 20S proteasome α-subunit (Fig. 7C). These data suggest that fibrillation and acquisition of the auxiliary proteins are not spontaneous consequences of the aggregate growth, rather they are closely linked to the microtubule-dependent inclusion-forming process.

B.2. Golgi fragmentation in the cells that produce spherical α-syn aggregates

As part of the effort to find the pathogenic aggregate species and their cellular targets, we have tested the hypothesis that formation of prefibrillar oligomeric α-syn causes Golgi fragmentation. This study was made possible by the establishment of the cell culture model system, in which the effects of monomer and different types of α-syn aggregates can be distinguished. The results of the study using this cell system are summarized. For details, see A2, Gosavi et al. Figures that are referenced in this section can be found in A2.

1. ***Association between Golgi fragmentation and the formation of prefibrillar α-syn aggregates.*** To investigate cellular consequences specific to α-syn aggregation, we have analyzed the morphological integrity of Golgi apparatus (GA) with respect to the α-syn aggregation states using an immunofluorescence microscopy with the antibody against a cis-Golgi-specific matrix protein GM130. In cells with diffuse α-syn staining, the GA has normal compact morphology near the nucleus (Fig. 3A). However, the cells with prefibrillar aggregates frequently show fragmentation and dispersion of the GA (Fig. 3B and C). Golgi fragmentation was found far more frequently in the population with the aggregates (88.9%) than in general population (11.5%) (Fig. 3E). To further determine if Golgi fragmentation is aggregation-induced event, cells with fragmented Golgi were counted at different α-syn expression conditions. Expression of a high-level of soluble α-syn did not affect the Golgi fragmentation. On the other hand, the Golgi fragmentation was significantly increased in the condition where prefibrillar aggregates formed with stable monomer levels (Fig. 3D). These results suggest that increase of α-syn aggregates, rather than the monomer, might be the cause of Golgi fragmentation.

2. ***Absence of correlation between Golgi fragmentation and fibrillar inclusion body.*** In contrast to the prefibrillar aggregates, no clear association was found between the fibrillar inclusions and the Golgi fragmentation. First, increase in Golgi fragmentation occurs before the appearance of fibrillar inclusions (Fig. 2B and 3F). Secondly, the size of the cell population that contains fragmented GA does not increase during the period when a sudden increase in the number of fibrillar inclusions takes place (Fig. 2B and 3F). Finally, fragmented GA was rarely observed in the cells with fibrillar inclusions. Instead,

two types of GA morphology were associated with fibrillar inclusions: in most cases, Golgi components were confined and dispersed inside the fibrillar inclusions (Fig. 7A), and occasionally, some cells maintained the compact, although slightly distorted, morphology of GA that surrounded the juxtanuclear fibrillar inclusions (Fig. 7B). The fact that Golgi fragmentation occurs before the formation of inclusions and that some cells maintain the compact Golgi structure despite the presence of inclusions suggests that the inclusions themselves may not be the direct cause of the morphological disruption of the GA. Rather, co-staining of the fibrillar inclusions with α-syn and Golgi marker suggests that the inclusions might be a consequence of the cell's attempt to remove abnormal protein aggregates and impaired organelles from the cytoplasm.

3. ***Juxtanuclear inclusion bodies may represent cellular response to toxic protein aggregation and impairment of organelles.*** Lysosomes and mitochondria, which normally tend to be dispersed in the cytoplasm, showed a rather localized pattern in the juxtanuclear region in the presence of the prefibrillar α-syn aggregates (Fig. 8A and C). These organelles showed no sign of fragmentation and appear to be functionally intact. EM study also showed the accumulation of fragmented Golgi (Fig. 9, box 1) and intact mitochondria in the juxtanuclear region (Fig. 9). In addition, autophagosomes and lysosomes can be found in this area at the early stage of inclusion formation (Fig. 9, box 2). Proteasomes and chaperone molecules were also accumulated near the nucleus in the cells with α-syn aggregates. It has been suggested that the juxtanuclear pericentriolar region serves as the main location in which both autophagic-lysosomal system and ubiquitin-proteasome system execute their degradation function to remove abnormal proteins and damaged organelles (Wigley et al., 1999; Kopito, 2000; Garcia-Mata et al., 2002). Thus, the localization of functional lysosomes and mitochondria in the juxtanuclear region may be the manifestation of cell's defense mechanisms against the protein aggregates. Together, these results suggest that the formation of α-syn aggregates trigger the action of cellular defense system, which is represented by the accumulation of these aggregates and impaired organelles in the juxtanuclear region along with the mitochondria, autophagosomes/lysosomes, and proteasomes.

B.3. Cytotoxic effects of prefibrillar α-syn aggregates

A cytotoxic effect of α-syn has been reported in several mammalian cell systems (Ostrerova et al., 1999; Saha et al., 2000; Iwata et al., 2001; Zhou et al., 2002). However, the nature of toxic species has not been determined. Since the formation of prefibrillar aggregates correlates with the disruption of Golgi apparatus (GA), a vital organelle of eukaryotic cells, we measured cell viability as a function of the aggregate formation. Increase of monomer, without forming aggregates, did not affect the viability (MOI 0-20) (Fig. 1*A* and Fig. 2*A*, day 3). In contrast, cell viability was significantly reduced when aggregates formed without increasing the monomer level (Fig. 1*A* and Fig. 2*A*, day3). Tight correlation between reduction in cell viability and α-syn aggregation was also found in the time-course study. Aggregates were formed at slower rates at lower MOIs (MOIs 20 and 50), and when they became apparent on the fourth day, the viability was reduced correspondingly (Fig. 1*A* and *B*). Like the Golgi fragmentation, reduction in cell viability occurred before the appearance of the fibrillar inclusions (Fig. 2*A*, day 3 at the MOI of 70, and see also Fig. 1*B* and *C*), implicating a cytotoxic effect of prefibrillar aggregates. In contrast, overexpression of GFP did not affect the cell viability in the same time period (Fig.

1*C*). These results suggest that the cytotoxic effect of α-syn depends on its ability to form aggregates, and that prefibrillar aggregates, rather than the fibrillar inclusion bodies, may be responsible for the toxicity.

Although the causal relationship between Golgi fragmentation and cell death is not clear at the moment, following observations support that Golgi fragmentation is probably at the upstream of the cell death process, rather than a mere consequence of the latter. First, Golgi fragmentation was found, without exception, in all dying cells that were stained with ethidium homodimer (EthD), whereas not all the cells with Golgi fragmentation were EthD-positive, though most were (Fig. 2*D*). This suggests that Golgi fragmentation precedes the membrane permeabilization in cell death process. Secondly, the same changes in the GA cannot be found in hydrogen peroxide-induced cell death, suggesting that the type of morphological changes in the GA found in association with α-syn aggregation is not a general consequence of cell death.

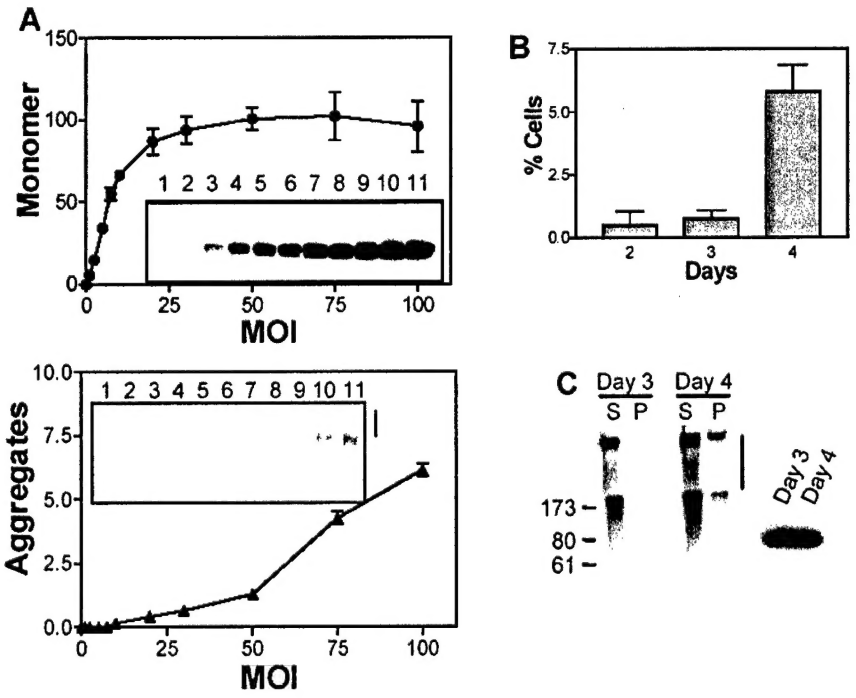

Fig. 1. Non-linear relationship between the production of monomeric α-syn and its aggregation. (***A***) COS-7 cells were infected with different amount of adenoviral vector (adeno/α-syn) carrying α-syn cDNA and incubated for three days, and the levels of monomers and aggregates were measure from detergent-soluble and insoluble fractions, respectively. Empty viral vector was added so as to make the total number of viral particles in each sample constant. Arbitrary optical density units are plotted in the graphs. Insets are the representative autoradiograms of the Western blotting using LB509 antibody and ^{125}I-labeled secondary antibody. Specific MOIs used in the Western analysis are: lane 1, 0; lane 2, 1; lane 3, 2.4; lane 4, 5; lane 5, 7.4; lane 6, 10; lane 7, 20; lane 8, 30; lane 9, 50; lane 10, 75; lane 11, 100. The vertical line on the right side of the inset indicates the stacking gel portion. (***B***) The percentages of cells that contain juxtanuclear inclusion bodies were calculated at the indicated time points. α-Syn was expressed at MOI of 75. Images were obtained from two optical sections to ensure the detection of inclusion bodies that are located in a different plane. (***C***) Fibrillar inclusions (P) and prefibrillar oligomers (S) were separated based on their sizes at day 3 and day 4, and analyzed by Western blotting. The left and right panels show the detergent-insoluble aggregates and soluble monomers, respectively. The vertical line indicates the stacking gel portion.

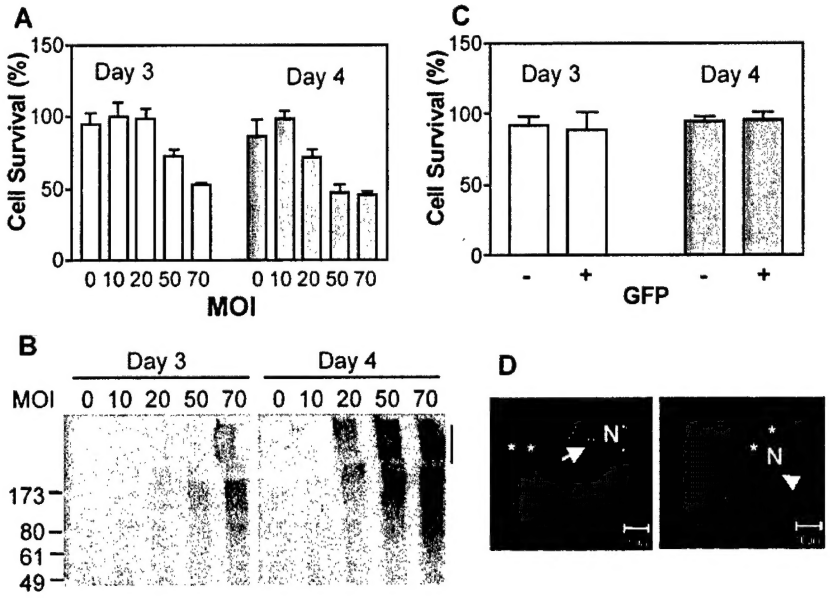

Fig. 2. Cytotoxic effect of α-syn is dependent on the aggregation and occurs before the formation of fibrillar inclusions. (***A***, ***B***) COS-7 cells were infected with adeno/α-syn at given MOIs (the total number of viral particles was adjusted to be equivalent by adding appropriate amount of empty viral vector), and each sample was subjected to the trypan blue exclusion assay (*A*) and Western blotting (*B*). The percentage of live cell number was calculated, with the non-expressor at day 3 as being 100%. The Western blotting was performed with the detergent-insoluble fractions. (***C***) Cell viability was analyzed in control-transfectants (-) or GFP-transfectants (+). The percentage of live cells was obtained, with the control-transfectants at day 3 as being 100%. (***D***) COS-7 cells were infected with adeno/α-syn at the MOI of 75 and stained with EthD (red) and anti-GM130 antibody (green) at day 3. EthD stains the nucleus of dying cells. Left image shows a dying cell with EthD-positive nucleus (N) and fragmented Golgi. All the EthD-positive cells analyzed in this study showed Golgi fragmentation. The image on the right shows an example of the cell with fragmented Golgi and EthD-negative nucleus (N). Note that live cells have EthD-negative nucleoplasms [two nucleoli (*) are stained per cell] and normal Golgi morphology. Scale bars, 10 μm

B.4. α-Syn aggregation causes microtubule dysfunction and neurite degeneration in neurons.

In the final year of the project, we investigated the underlying mechanism of α-syn-induced Golgi fragmentation. It has previously been shown that drug-induced depolymerization of the MT leads to Golgi fragmentation with characteristic features. For example, cis/trans and matrix/non-matrix Golgi components are still co-localized even after the fragmentation (Fig. 3A) (Thyberg and Moskalewski, 1999) and accumulate at the transitional endoplasmic reticulum sites (tER) (Fig. 3C) (Cole et al., 1996); Sec13 is a standard marker for these sites. To compare patterns of Golgi fragmentation, COS-7 cells were either infected with the adenoviral vector adeno/α-syn, or treated with nocodazole, a MT-depolymerizing agent. The cells were then immunostained to detect the *cis*-Golgi matrix protein GM130 and the *trans*-Golgi membrane protein TGN46. Another set of cells were transfected with Sec13-YFP before the treatments to visualize the tER. As shown in Fig. 3, Golgi fragmentation in α-syn overexpressing cells displays typical features of the fragmentation induced in nocodazole-treated cells; cis-matrix

protein and trans-non-matrix proteins co-segregated and were redistributed to the tER sites. These results suggest that Golgi fragmentation in α-syn overexpressing cells may be a manifestation of a dysfunctional MT system.

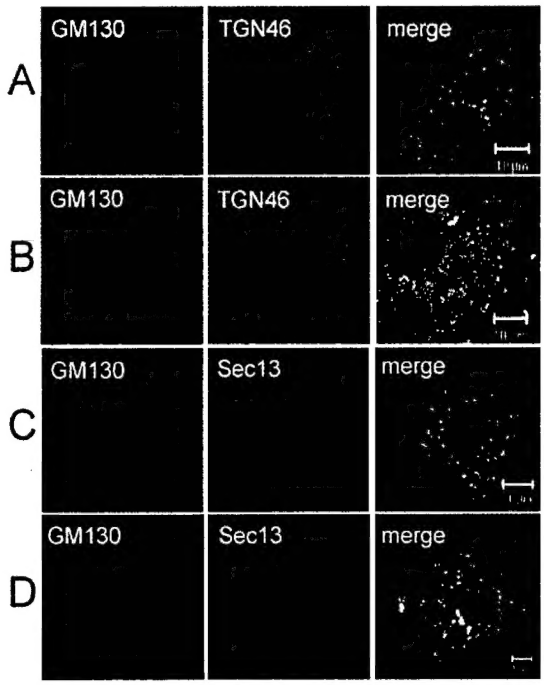

Fig. 3. Golgi fragmentation pattern of α-syn overexpressing cells is similar to that of MT-disrupted cells. COS-7 cells were either treated with 5 μg/mL nocodazole (A, C) or infected with adeno/α-syn (B, D). GM130 and TGN46 were visualized by immunofluorescence staining, and Sec13 was visualized by the expression of Sec13-YFP fusion protein.

To study the effects of α-syn overproduction on MT function and its downstream effects in post-mitotic neuronal cells, we first quantified Golgi fragmentation in differentiated SH-SY5Y human neuroblastoma cells at different levels of α-syn expression. Golgi fragmentation occurs in cells with a high-level of α-syn expression, often with punctate α-syn deposits (Fig. 4A). Similar to our previous results in COS-7 cells (Gosavi et al., 2002), the extent of Golgi fragmentation has a non-linear relationship with the α-syn expression level; the threshold α-syn expression level for Golgi fragmentation is approximately that required for aggregate formation (Fig. 4B and C). This result suggests that aggregation of α-syn may lead to Golgi fragmentation in neuronal cell types. Overexpression of β-galactosidase did not cause Golgi fragmentation (Fig. 4B), indicating that it is not a general effect of protein overexpression. The dispersion of Golgi fragments to the tER was also found in differentiated neuroblastoma cells overexpressing α-syn (Fig. 4D), indicating that MT dysfunction is the underlying cause of Golgi fragmentation in these cells. To further confirm this observation in primary neurons, we examined the Golgi morphology in a primary culture of DRG neurons after overexpression of α-syn. These neurons also show severe dispersion of the Golgi apparatus (Fig. 5B-D), and in some cases, Golgi fragments are dispersed even into the neurites (Fig. 5D). Another feature that is consistently observed in these cells is neuritic degeneration that is characterized by neuritic spheroid-like swellings and shortening (Fig. 5B-D). These findings support the hypothesis that α-syn overproduction, probably via

aggregation, causes MT dysfunction, leading to the downstream cellular impairment, such as Golgi fragmentation and neuritic degeneration.

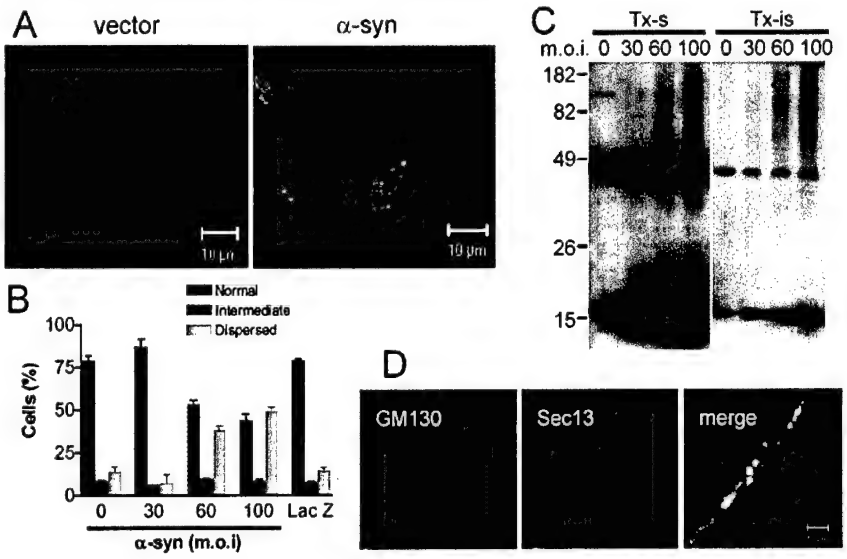

Fig. 4. Golgi fragmentation in differentiated SH-SY5Y cells. (A) Cells were infected with either empty vector (left) or adeno/α-syn (right). Red: α-syn, green: GM130, blue: nuclei (B) Quantitative analysis of Golgi morphology at different levels of α-syn expression. Total amount of viral vector was normalized with empty vector. (C) Aggregation of α-syn at different expression levels. Tx-s: Triton-soluble fraction, Tx-is: Triton-insoluble fraction (D) Co-localization of fragmented Golgi and Sec13 in α-syn overexpressing cells. GM130 and Sec13 were visualized as in Fig. 3.

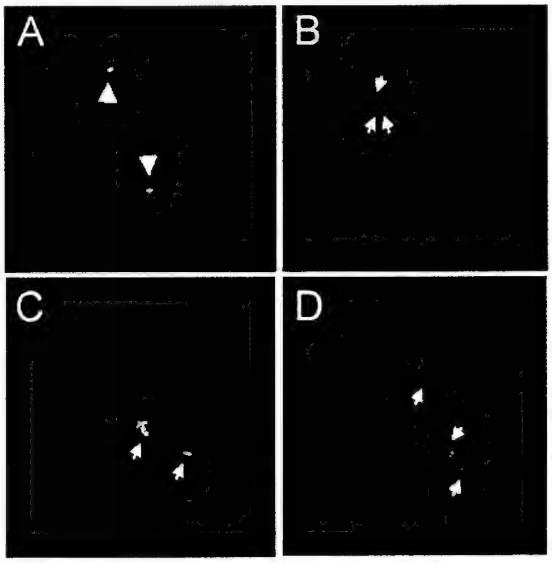

Fig. 5. Golgi fragmentation and neuritic degeneration in α-syn overexpressing DRG neurons. (A) Empty vector-infected neurons. Arrowheads indicate Golgi apparatus with normal morphology. (B-D) Neurons overexpressing α-syn. Arrows indicate dispersed Golgi fragments. Note that these neurons also exhibit degenerative neuritic morphology.

To further characterize the neuritic phenotype, we expressed α-syn at different levels in differentiated neuroblastoma cells and analyzed the neuritic morphology. Unlike normal cells, which have long and straight processes (Fig. 6A), the cells overexpressing α-syn lack these processes; instead they show thickened and irregular shapes at the former roots of the processes (Fig. 6B). The percentage of cells with this type of neuritic degeneration increases with increasing levels of α-syn expression, whereas overexpression of β-galactosidase has no effect on the neurites (Fig. 6C). Spherical α-syn-positive aggregates are generally found at the tip of the degenerating neurites (Fig. 7 and Fig. 8). These α-syn aggregates invariably contain tubulins (Fig. 7). At least some of these are post-translationally modified tubulins, such as acetylated and poly-glutamylated tubulins (Fig. 7C and D). Acetylation of tubulin is associated with stable MTs, and occurs after the tubulins are polymerized into MTs (Westermann and Weber, 2003). Thus, these α-syn/tubulin co-aggregates may be in part derived from the disruption of MT polymers. Indeed, most of the cells that overexpress α-syn have a drastically reduced MT network (Fig. 6-8) compared to normal cells (Fig. 6A). α-Syn/tubulin co-aggregation and MT dysfunction seem to be the cause, rather than the consequence, of neuritic degeneration, because some cells that have yet to undergo neuritic degeneration show small punctate co-aggregates of α-syn/tubulin in the neuritic processes (Fig. 7E). Co-localization of tubulin with α-syn aggregates suggests an altered solubility of tubulin in α-syn overexpressing cells. To test this, we examined the detergent solubility of tubulin at different levels of α-syn expression using a cold buffer containing 1% Tronton-X100, in which normal MTs are depolymerized to soluble tubulins. In agreement with the immunofluorescence data, overexpression of α-syn elevated the levels of detergent-insoluble tubulins, while most tubulins were extracted into the soluble fractions (Fig. 7F).

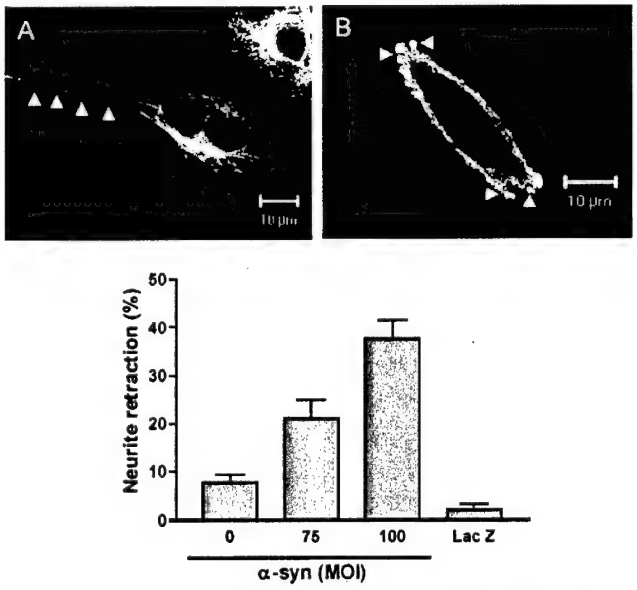

Fig. 6. MT disruption and neuritic degeneration in differentiated SH-SY5Y cells. Cells were infected with either empty vector (A) or adeno/α-syn (B), and immunostained for β-tubulin. Control cells show normal processes and MT network (A), whereas α-syn overexpressing cells show retracted neurites and little MT network (B). (C) Quantitative analysis of neuritic degeneration at different levels of α-syn expression. Total amount of viral vector was normalized with empty vector.

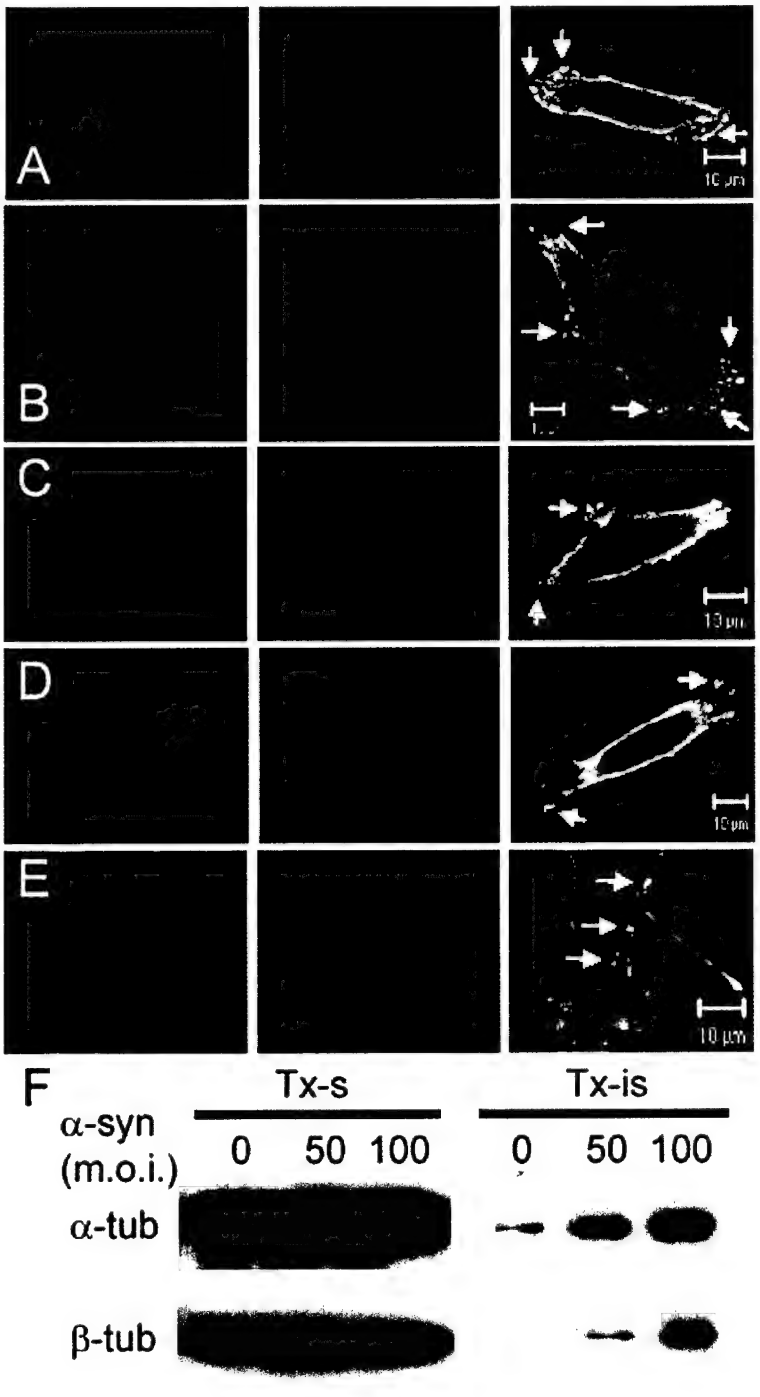

Fig. 7. Co-localization of tubulin with α-syn aggregates. Differentiated SH-SY5Y cells overexpressing α-syn were immunostained for α-syn (red) and various tubulins (green): (A, E) α-tubulin, (B) β-tubulin, (C) acetylated tubulin, and (D) polyglutamylated tubulin. α-Syn aggregates (arrows) are found at the tip of the degenerating neurites (A-D) and in some cells, within the neuritic processes (E). (F) Triton-soluble (Tx-s) and –insoluble (Tx-is) tubulins were analyzed with Western blotting at different levels of α-syn expression.

To study the effects of α-syn aggregates on other components of the MT system, we examined the distribution of the MT motor proteins. The MT system uses two types of molecular motors depending on the direction of movement: the plus-end directed motors and the minus-end directed motors transport cargo towards the plus-end and the minus-end of the MTs, respectively (Goldstein and Yang, 2000). In this study, we have analyzed the distribution of two plus-end motor components, kinesin heavy chain (KHC) and KIF3A, and two minus-end motor components, $p150^{Glued}$ and p50/dynamitin. We have found that only the minus-end motor subunits co-localize with α-syn aggregates, while the plus-end motor subunits are almost completely excluded from the aggregates (Fig. 8). It has been suggested that protein aggregates are transported by minus-end directed motors to form higher-order inclusion bodies (Kopito, 2000). Our study confirms that α-syn aggregates are handled by a specific motor system, and thus may lead to its impairment when the system is loaded beyond its capacity.

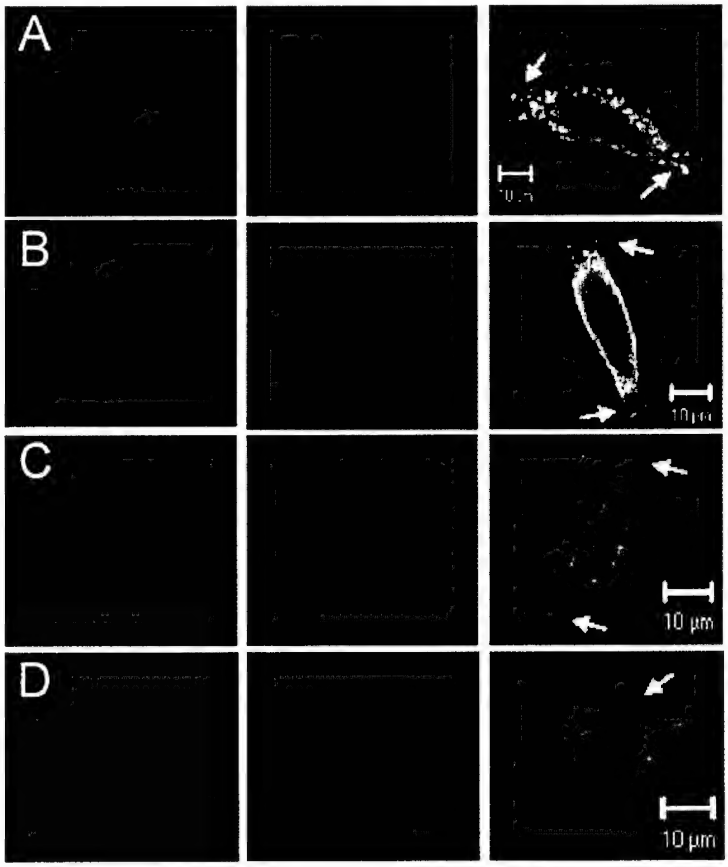

Fig. 8. Co-localization of minus-end directed MT motors with α-syn aggregates. Differentiated SH-SY5Y cells overexpressing α-syn were immunostained for α-syn (red) and various MT motor subunits (green). Two minus-end directed motor components, p50/dynamitin (A) and $p150^{Glued}$ (B), and two plus-end directed motor components, KHC (C) and KIF3A (D), are shown. Arrows indicate spherical α-syn aggregates. Note that only the minus-end directed motors, not the plus-end directed motors, co-localize with α-syn aggregates.

B.5. Trafficking defects in cells with α-syn aggregates

To further characterize the effects of microtubule dysfunction in α-syn-overexpressing cells, we investigated the effects of α-syn overexpression on the microtubule-dependent trafficking. The temperature-sensitive mutant form of the vesicular stomatitis virus G protein (VSV-G) is a widely-used model protein in studying trafficking through the biosynthetic pathway (Pepperkok et al., 1993; Scales et al., 1997; Seemann et al., 2000). Here, we studied the trafficking property of this protein using an adenoviral vector bearing the GFP-tagged VSV-G gene. As shown in Fig. 9, VSV-G fails to fold properly and accumulates in ER at the restrictive temperature of 39.5°C (t = 0). But after the cells are transferred to the permissive temperature of 31.5°C, VSV-G folds rapidly and is transported progressively from the ER through the GA (t = 20 min) to the plasma membrane (PM; t = 60 min) in a time-dependent manner.

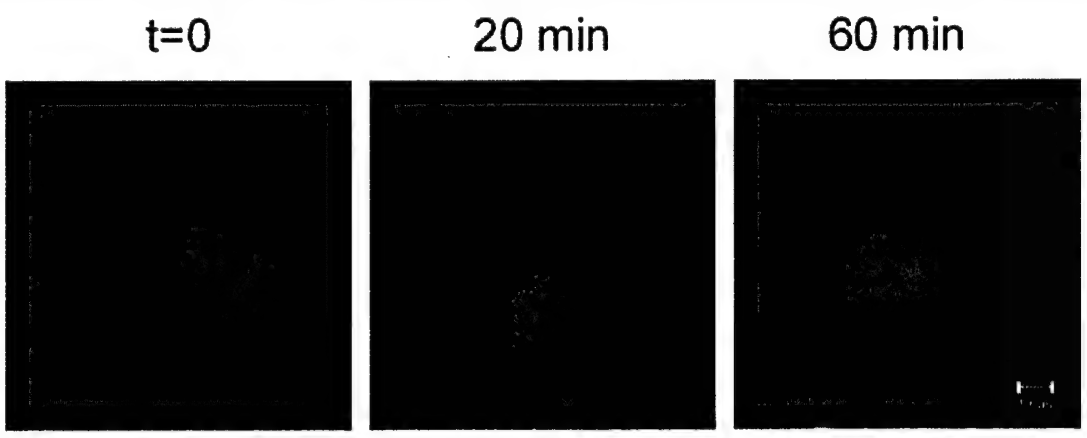

Fig. 9. Trafficking of VSVG-GFP in COS-7 cells. (**A**) Representative cells at three time points. At the permissive temperature, VSVG-GFP moves from the ER (t=0) to the GA (20 min) and then to the cell surface (60 min). *green*: total VSVG-GFP

To examine the effects of α-syn aggregation on VSV-G trafficking, we performed an experiment in which distribution of VSVG-GFP was visually observed. VSVG-GFP was expressed in COS-7 cells overexpressing α-syn at a restrictive temperature for 6.5 h, and then at a permissive temperature for 60 min, after which the cells were fixed, stained with α-syn antibody, and examined with confocal microscopy. The cells with diffuse α-syn expression without apparent aggregation often show typical VSV-G distribution; intense Golgi localization with clear cell surface expression (Fig. 10). On the other hand, the cells with noticeable spherical α-syn aggregates tend to show little VSV-G protein on the cell surface and dispersed cytoplasmic distribution (Fig. 10). This suggests that the trafficking of VSV-G may be impaired in cells with α-syn aggregates, thus supporting the conclusion that α-syn aggregation causes microtubule dysfunction.

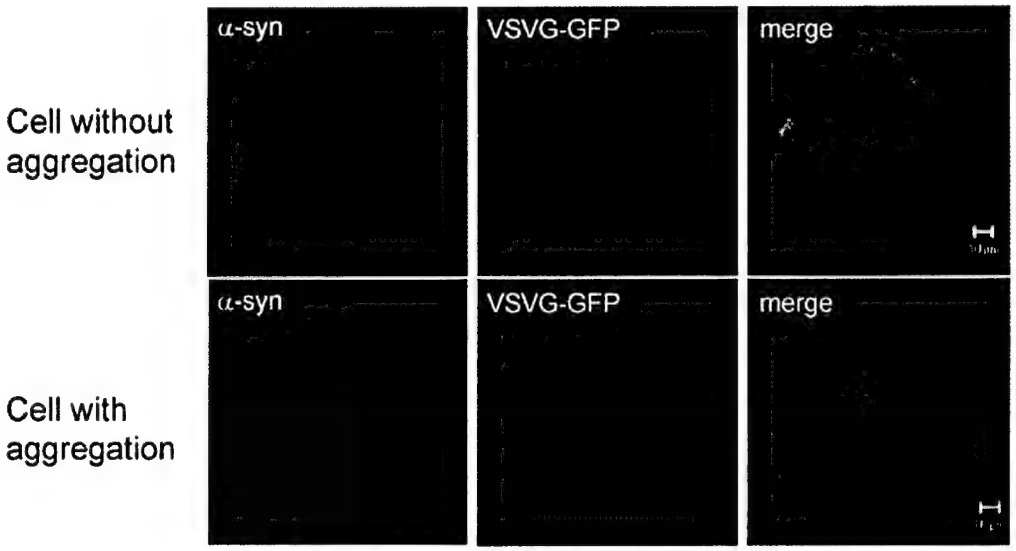

Fig. 10. Effect of α-syn aggregation on VSVG-GFP export in COS-7 cells overexpressing α-syn. Representative cell without apparent aggregation (top) exports VSVG-GFP to the cell surface, while a representative cell with spherical aggregates (bottom) shows little VSVG-GFP expressed on the cell surface. *red*: α-syn, *green*: VSVG-GFP

C. Key Research Accomplishments

- Biochemical fractionation method to separate the α-syn aggregate subspecies from the cytoplasm has been established.
- The fractionation and EM studies show that the juxtanuclear inclusion bodies are filled with α-syn fibrils and that at least two different prefibrillar spherical aggregates are formed in the course of fibrillation.
- Time-course and microtubule-disruption experiments show that spherical aggregates are the precursors for fibrillar inclusion bodies.
- α-Syn fibrillation in cells is tightly coordinated with the microtubule-dependent inclusion-forming process.
- Formation of prefibrillar oligomeric α-syn aggregates is associated with Golgi fragmentation, suggesting the prefibrillar intermediates as being pathogenic species.
- Fibrillar inclusion bodies seem to be a consequence of cellular effort to remove toxic protein aggregates and damaged organelles from cytoplasm.
- Deleterious effects of α-syn aggregation on Golgi fragmentation and cell viability were confirmed in post-mitotic neuronal cells.

- α-Syn aggregation causes the disruption of the microtubule network and the intracellular trafficking, leading to Golgi fragmentation and neuritic degeneration.

D. Reportable Outcomes

Publications

Lee H-J, Lee S-J (2002) Characterization of cytoplasmic α-synuclein aggregates: Fibril formation is tightly linked to the inclusion forming process in cells. *J. Biol. Chem.* 277, 48976-48983

Gosavi N, Lee H-J, Lee JS, Patel S, Lee S-J (2002) Golgi Fragmentation Occurs in the Cells with prefibrillar α-Synuclein aggregates and Precedes the Formation of Fibrillar Inclusion. *J. Biol. Chem.* 277, 48984-48992

Lee S-J (2003) α-Synuclein aggregation: a link between mitochondrial defects and Parkinson's disease? *Antiox. Redox Signal.* 5, 337-348

Khoshaghideh F, Lee H-J, Lee S, Lee S-J (2004) alpha-synuclein aggregation, microtubule dysfunction, and neuritic degeneration in neuronal models of synucleinopathies. *Submitted*

Presentations

Lee S-J (Jun. 2002) Golgi fragmentation and reduced cell viability in cells with prefibrillar α-synuclein aggregates. *FASEB Summer Conference on "Amyloids and Other Abnormal Protein Folding Processes"* Snowmass Village, CO

Lee H-J, Lee S-J (Jun. 2002) Isolation and characterization of α-synuclein aggregates in cells exposed to mitochondrial inhibitors. *FASEB Summer Conference on "Amyloids and Other Abnormal Protein Folding Processes"* Snowmass Village, CO

Lee H-J, Lee S-J (Nov. 2002) Isolation and characterization of aggregates from cells that overexpress α-synuclein. *Society for Neuroscience 32nd annual meeting*, Orlando, FL

Gosavi N, Lee H-J, Lee JS, Patel S, Lee S-J (Nov. 2002) Golgi fragmentation and reduced cell viability by prefibrillar α-synuclein aggregates. *Society for Neuroscience 32nd annual meeting*, Orlando, FL

Khoshaghideh F, Lee H-J, Lee S, Lee S-J (Jun. 2004) Microtubule dysfunction, neuritic degeneration, and Golgi fragmentation in differentiated neuroblastoma cells overproducing alpha-synuclein. *FASEB Summer Conference on "Protein misfolding, amyloid and conformational disease"* Snowmass Village, CO

Lee S-J, Khoshaghideh F, Lee S, Lee H-J (Oct. 2004, scheduled) Alpha-synuclein aggregation leads to microtubule dysfunction, neuritic degeneration, and Golgi fragmentation. *Society for Neuroscience 34th annual meeting*, San Diego, CA

Funding applied for based on work supported by this award

2003-2005 Michael J. Fox Foundation for Parkinson's Research (Awarded)
Title: Study of the metabolism and aggregation of α-synuclein in parkin-depleted neuronal cells (The fractionation of α-synuclein aggregates, that was established in year 1, is a key component of this proposal.)

2004-2006 Michael J. Fox Foundation for Parkinson's Research (Awarded)
Title: Intracellular trafficking dysfunction caused by alpha-synuclein aggregation (This project is to test the hypothesis that alpha-synuclein aggregation leads to microtubule dysfunction and intracellular trafficking defects. This hypothesis was formulated based on the results of the current study.)

E. Conclusions

A growing body of evidence suggests that aggregation of α-syn might be the fundamental cause of many neurodegenerative diseases. Several groups have developed cell culture models to study the cytotoxic effect of α-syn, and some of them indeed have observed enhanced cell death when α-syn, especially its mutant forms, was overexpressed (Ostrerova et al., 1999; Saha et al., 2000; Iwata et al., 2001; Zhou et al., 2002). However, the link between α-syn aggregation and cell death has not been clearly addressed in these model systems, nor are the molecular mechanisms underlying the toxicity known. We have begun to address these issues in a COS-7 cell model, and found that α-syn aggregation/oligomerization is tightly associated with Golgi fragmentation and cell death (Gosavi et al., 2002). More recently, fragmentation of the GA has been confirmed in a neuronal cell model, and the mode of Golgi fragmentation appears identical to that caused by microtubule-disrupting agents; dispersed Golgi fragments are localized to the transitional endoplasmic reticulum. Indeed, we found that α-syn aggregation led to the disruption of the microtubule network in neuronal models. Microtubule disruption then caused intracellular trafficking impairment and neurite degeneration. These data identify microtubule dysfunction as being the link between α-syn aggregation and neurodegeneration.

Recent studies show that the microtubule transport system also plays a role in inclusion body formation, as part of the cellular response to the aggregation of misfolded proteins (Johnston et al., 1998; Garcia-Mata et al., 1999; Johnston et al., 2000). Aggregation of proteins could occur anywhere in the cytoplasm, resulting in many small aggregate particles scattered throughout the cell. These particles are deposited in the pericentriolar region, adjacent to the microtubule-organizing center, by retrograde transport on microtubules. These microtubule-dependent deposits of aggregates are called aggresomes (Johnston et al., 1998) and may explain the biogenesis of inclusion bodies found in neurological diseases, such as Lewy bodies in PD. The microtubule-dependent nature of inclusion formation suggests that extensive protein aggregation in neurons may place a tremendous burden on the microtubule transport system, causing it to malfunction. In the first year of the project, we have shown that small α-syn oligomers are transported on the microtubules and deposit to form inclusion bodies (Lee and Lee, 2002). In addition, our current data indicate that α-syn overproduction causes the disruption of neuronal MT network, probably via aggregation. This, in turn, leads to downstream degenerative changes,

such as neuritic degeneration and Golgi fragmentation, which are common pathological features shared by many human neurodegenerative diseases (Gonatas et al., 1998). Determining the precise mechanism by which abnormal α-syn disturbs MT integrity will provide insight into the early pathogenic mechanism of PD and other synucleinopathies.

F. References

Auluck PK, Chan HY, Trojanowski JQ, Lee VM, Bonini NM (2002) Chaperone suppression of alpha-synuclein toxicity in a Drosophila model for Parkinson's disease. Science 295:865-868.

Cole NB, Sciaky N, Marotta A, Song J, Lippincott-Schwartz J (1996) Golgi dispersal during microtubule disruption: regeneration of Golgi stacks at peripheral endoplasmic reticulum exit sites. Mol Biol Cell 7:631-650.

Conway KA, Rochet JC, Bieganski RM, Lansbury PT, Jr. (2001) Kinetic stabilization of the alpha-synuclein protofibril by a dopamine- alpha-synuclein adduct. Science 294:1346-1349.

Conway KA, Lee S-J, Rochet JC, Ding TT, Williamson RE, Lansbury PT, Jr. (2000) Acceleration of oligomerization, not fibrillization, is a shared property of both alpha-synuclein mutations linked tc early-onset Parkinson's disease: implications for pathogenesis and therapy. Proc Natl Acad Sci U S A 97:571-576.

Garcia-Mata R, Gao YS, Sztul E (2002) Hassles with Taking Out the Garbage: Aggravating Aggresomes. Traffic 3:388-396.

Garcia-Mata R, Bebok Z, Sorscher EJ, Sztul ES (1999) Characterization and dynamics of aggresome formation by a cytosolic GFP- chimera. J Cell Biol 146:1239-1254.

Giasson BI, Duda JE, Quinn SM, Zhang B, Trojanowski JQ, Lee VM-Y (2002) Neuronal alpha-Synucleinopathy with Severe Movement Disorder in Mice Expressing A53T Human alpha-Synuclein. Neuron 34:521-533.

Goldstein LS, Yang Z (2000) Microtubule-based transport systems in neurons: the roles of kinesins and dyneins. Annu Rev Neurosci 23:39-71.

Gonatas NK, Gonatas JO, Stieber A (1998) The involvement of the Golgi apparatus in the pathogenesis of amyotrophic lateral sclerosis, Alzheimer's disease, and ricin intoxication. Histochem Cell Biol 109:591-600.

Gosavi N, Lee H-J, Lee JS, Patel S, Lee S-J (2002) Golgi Fragmentation Occurs in the Cells with Prefibrillar alpha - Synuclein Aggregates and Precedes the Formation of Fibrillar Inclusion. J Biol Chem 277:48984-48992.

Hardy J, Gwinn-Hardy K (1998) Genetic classification of primary neurodegenerative disease. Science 282:1075-1079.

Ii K, Ito H, Tanaka K, Hirano A (1997) Immunocytochemical co-localization of the proteasome in ubiquitinated structures in neurodegenerative diseases and the elderly. J Neuropathol Exp Neurol 56:125-131.

Iwata A, Maruyama M, Kanazawa I, Nukina N (2001) alpha-Synuclein affects the MAPK pathway and accelerates cell death. J Biol Chem 276:45320-45329.

Johnston JA, Ward CL, Kopito RR (1998) Aggresomes: a cellular response to misfolded proteins. J Cell Biol 143:1883-1898.

Johnston JA, Dalton MJ, Gurney ME, Kopito RR (2000) Formation of high molecular weight complexes of mutant Cu, Zn- superoxide dismutase in a mouse model for familial amyotrophic lateral sclerosis. Proc Natl Acad Sci U S A 97:12571-12576.

Kopito RR (2000) Aggresomes, inclusion bodies and protein aggregation. Trends Cell Biol 10:524-530.

Lee H-J, Lee S-J (2002) Characterization of Cytoplasmic alpha -Synuclein Aggregates. FIBRIL FORMATION IS TIGHTLY LINKED TO THE INCLUSION-FORMING PROCESS IN CELLS. J Biol Chem 277:48976-48983.

Ostrerova N, Petrucelli L, Farrer M, Mehta N, Choi P, Hardy J, Wolozin B (1999) alpha-Synuclein shares physical and functional homology with 14-3-3 proteins. J Neurosci 19:5782-5791.

Pepperkok R, Scheel J, Horstmann H, Hauri HP, Griffiths G, Kreis TE (1993) Beta-COP is essential for biosynthetic membrane transport from the endoplasmic reticulum to the Golgi complex in vivo. Cell 74:71-82.

Saha AR, Ninkina NN, Hanger DP, Anderton BH, Davies AM, Buchman VL (2000) Induction of neuronal death by alpha-synuclein [In Process Citation]. Eur J Neurosci 12:3073-3077.

Scales SJ, Pepperkok R, Kreis TE (1997) Visualization of ER-to-Golgi transport in living cells reveals a sequential mode of action for COPII and COPI. Cell 90:1137-1148.

Seemann J, Jokitalo EJ, Warren G (2000) The role of the tethering proteins p115 and GM130 in transport through the Golgi apparatus in vivo. Mol Biol Cell 11:635-645.

Spillantini MG, Crowther RA, Jakes R, Hasegawa M, Goedert M (1998) alpha-Synuclein in filamentous inclusions of Lewy bodies from Parkinson's disease and dementia with lewy bodies. Proc Natl Acad Sci U S A 95:6469-6473.

Thyberg J, Moskalewski S (1999) Role of microtubules in the organization of the Golgi complex. Exp Cell Res 246:263-279.

Trojanowski JQ, Goedert M, Iwatsubo T, Lee VM (1998) Fatal attractions: abnormal protein aggregation and neuron death in Parkinson's disease and Lewy body dementia [see comments]. Cell Death Differ 5:832-837.

Westermann S, Weber K (2003) Post-translational modifications regulate microtubule function. Nat Rev Mol Cell Biol 4:938-947.

Wigley WC, Fabunmi RP, Lee MG, Marino CR, Muallem S, DeMartino GN, Thomas PJ (1999) Dynamic association of proteasomal machinery with the centrosome. J Cell Biol 145:481-490.

Zhou W, Schaack J, Zawada WM, Freed CR (2002) Overexpression of human alpha-synuclein causes dopamine neuron death in primary human mesencephalic culture. Brain Res 926:42-50.

List of personnel who worked on the study:
Seung-Jae Lee, Ph.D., Principal Investigator
He-Jin Lee, Ph.D., Post-Doc
Nirmal Gosavi, Research Assistant
Billy Wong, Research Assistant
Stephen Lee, Research Assistant

THE JOURNAL OF BIOLOGICAL CHEMISTRY Vol. 277, No. 50, Issue of December 13, pp. 48976–48983, 2002
Printed in U.S.A.

Characterization of Cytoplasmic α-Synuclein Aggregates

FIBRIL FORMATION IS TIGHTLY LINKED TO THE INCLUSION-FORMING PROCESS IN CELLS*

Received for publication, August 9, 2002, and in revised form, September 9, 2002
Published, JBC Papers in Press, September 25, 2002, DOI 10.1074/jbc.M208192200

He-Jin Lee and Seung-Jae Lee‡

From the The Parkinson's Institute, Sunnyvale, California 94089

The α-synuclein fibrillation process has been associated with the pathogenesis of several neurodegenerative diseases. Here, we have characterized the cytoplasmic α-synuclein aggregates using a fractionation procedure with which different aggregate species can be separated. Overexpression of α-synuclein in cells produce two distinct types of aggregates: large juxtanuclear inclusion bodies and small punctate aggregates scattered throughout the cytoplasm. Biochemical fractionation results in an inclusion-enriched fraction and two small aggregate fractions. Electron microscopy and thioflavin S reactivity of the fractions show that the juxtanuclear inclusion bodies are filled with amyloid-like α-synuclein fibrils, whereas both the small aggregate fractions contain non-fibrillar spherical aggregates with distinct size distributions. These aggregates appear sequentially, with the smallest population appearing the earliest and the fibrillar inclusions the latest. Based on the structural and kinetic properties, we suggest that the small spherical aggregates are the cellular equivalents of the protofibrils. The proteins that co-exist in the Lewy bodies, such as proteasome subunit, ubiquitin, and hsp70 chaperone, are present in the fibrillar inclusions but absent in the protofibrils, suggesting that these proteins may not be directly involved in the early aggregation stage. As predicted in the aggresome model, disruption of microtubules with nocodazole reduced the number of inclusions and increased the size of the protofibrils. Despite the increased size, the protofibrils remained non-fibrillar, suggesting that the deposition of the protofibrils in the juxtanuclear region is important in fibril formation. This study provides evidence that the cellular fibrillation also involves non-fibrillar intermediate species, and the microtubule-dependent inclusion-forming process is required for the protofibril-to-fibril conversion in cells.

A group of human neurodegenerative diseases, such as Parkinson's disease (PD),[1] dementia with Lewy bodies (LBs), and multiple system atrophy, are characterized by cytoplasmic inclusion bodies that are mainly composed of α-synuclein fibrils (1, 2). Although direct role of fibrils and the inclusion bodies in the disease pathogenesis is the subject of intense debate, an increasing body of evidence suggests that the *processes* of fibrillation and inclusion formation are closely related to the disease mechanism. First, two missense mutations (A53T and A30P) that are responsible for the familial PD has been identified in α-synuclein gene (3, 4), and the mutant proteins have greater propensity for the self-association and aggregation than the wild type protein (5–7). Indeed, both mutations accelerated the formation of the pre-fibrillar oligomers *in vitro*, whereas the fibril formation was slowed by one of the mutations (7, 8). Second, transgenic animal models that were generated by the overexpression of human α-synuclein developed neuronal cytoplasmic inclusion bodies along with neuronal cell loss and behavioral defects (9–13). Some of these animals produce fibrillar inclusions (9, 12), but others generate only the granular aggregates (10). In a rat Parkinson's model, established by a systemic administration of rotenone, nigrostriatal degeneration and the motor symptoms were also accompanied by α-synuclein-positive inclusion bodies (14). Therefore, the cellular mechanism of α-synuclein aggregation is likely to be linked to at least some aspects of the disease process. Although the process of α-synuclein fibril formation has been implicated in the pathogenesis of PD by genetic and biochemical evidence, the exact mechanism by which the processes of α-synuclein fibrillation and inclusion body formation contribute to neurodegeneration is currently unknown.

In dilute solution, α-synuclein does not have stable structure (15) except for some residual helical structure in the N terminus of the protein (16). Fibrillation of α-synuclein is a nucleation-dependent process (17) and is initiated by acquiring a partially folded conformation (18), which is subsequently stabilized by self-association (19). Prior to the formation of the fibril, the end product of the process, several non-fibrillar oligomeric aggregates, or protofibrils, were identified (20). Earliest and most common protofibrillar species are in a spherical shape with average height of 4.2 nm in case of wild type protein (21). The spherical protofibrils are thought to undergo head-to-tail associations to form elongated chain-like (22), and ring-like protofibrillar species (21). In their search for a potential pathogenic mechanism for α-synuclein protofibrils, Lansbury and colleagues (23, 24) demonstrated that only protofibrillar α-synuclein bind tightly and permeabilize synthetic vesicles in a size-selective manner, suggesting membrane disruption via a pore-like mechanism. This hypothesis is supported by the findings that the two pathogenic mutations (A53T and A30P) promote the formation of annular pore-like protofibrils (25) and result in an increased permeabilization activity relative to the wild type protein (24). Although some of the basic processes of α-synuclein aggregation, including the protofibrils with different morphologies, have been characterized *in vitro*, little is known about the fibrillation process or the intermediate protofibrillar species in cells.

* This work was supported by the U. S. Army Medical Research Acquisition Activity (DAMD17-02-0171) and the Abramson Family Foundation. The costs of publication of this article were defrayed in part by the payment of page charges. This article must therefore be hereby marked "*advertisement*" in accordance with 18 U.S.C. Section 1734 solely to indicate this fact.

‡ To whom correspondence should be addressed: The Parkinson's Institute, 1170 Morse Ave., Sunnyvale, CA 94089. Tel.: 408-542-5642; Fax: 408-734-8522; E-mail: slee@thepi.org.

[1] The abbreviations used are: PD, Parkinson's Disease; LB, Lewy body; m.o.i., multiplicity of infection; EM, electron microscopy; PBS, phosphate-buffered saline; SB, 1× Laemmli sample buffer; fr, fraction.

To understand the mechanism of α-synuclein aggregation in cells, the following questions need to be addressed: (i) What is the end product of α-synuclein aggregation process in cells? (*i.e.* is it the fibril or other aggregate form?) (ii) What are the intermediates that proceed α-synuclein fibrillation in cells? (iii) Is the fibrillation process linked to the inclusion formation process, and if so, how? Here, using a combination of biochemical fractionation, immunofluorescence labeling, and electron microscopy (EM), we show that cells produce inclusion bodies that are filled with α-synuclein fibrils. Before the appearance of the fibrillar inclusions, small non-fibrillar aggregates are formed, and the basic properties of these aggregates suggest that they are the cellular equivalent of the protofibrils. Our study also provides evidence that the inclusion-forming process, which is characterized by the transport of α-synuclein protofibrils and other cellular components to the pericentriolar region, is required for the conversion of protofibrils to fibrils.

MATERIALS AND METHODS

Expression of Human α-Synuclein and Induction of Aggregation—Transformed African monkey kidney cell line COS-7 was maintained in Dulbecco's modified Eagle's medium (HyClone Laboratories, Inc., Logan, UT) with 10% fetal bovine serum (HyClone Laboratories, Inc.) in a 37 °C/5% CO_2 humidified incubator. To express α-synuclein, COS-7 cells were split on 100-mm tissue culture dishes 1 day prior to infection to obtain ~90% confluence on the day of infection. For infection, recombinant adenoviral vector (26) was added to each dish at a multiplicity of infection (m.o.i.) of 75. After 90 min of incubation at 37 °C, 9 ml of fresh medium was added and the cells were maintained at 37 °C. The cells were then split the next day to ~40% confluency and maintained for another 48 h or as indicated. Note that, in our culture condition, the time course of aggregation varies depending on the size of the culture dish used. For example, cells cultured in a 100-mm dish show more rapid aggregation than the cells in smaller dishes.

Fractionation of α-Synuclein Aggregates from COS-7 Cells—COS-7 cells expressing α-synuclein were washed twice with cold phosphate-buffered saline (PBS) before addition of buffer T (20 mM Tris, pH 7.4, 25 mM KCl, 5 mM $MgCl_2$, 0.25 M sucrose, 1% Triton X-100, protease inhibitor mixture (Sigma)) to each dish. After a 5-min incubation at room temperature, the supernatant containing Triton-soluble proteins was carefully removed from plates. After gentle washing of dishes with PBS, the Triton-insoluble materials were scraped in buffer N (0.1 M Na_2CO_3, pH 11.5, protease inhibitor mixture), resuspended by repeated pipetting, and incubated on ice for 5 min. The extract was then centrifuged at 80 × *g* for 10 min. The pellet containing big inclusions was resuspended in 1× Laemmli sample buffer (SB) for Western blot analysis, in PBS for immunofluorescence staining, or in 0.1 M phosphate buffer for EM. The supernatant containing small aggregates was then overlaid onto a discontinuous density gradient of 2.5%, 25%, and 35% iodixanol solutions (3:3:1, v/v) in buffer T and centrifuged at 50,000 × *g* for 30 min. The fractions were obtained from the top of the gradient, diluted with 2 volumes of PBS, and centrifuged at 16,000 × *g* for 10 min. The pellets from fractions were then resuspended in 1× SB for Western blot analysis, in PBS for immunofluorescence staining, or in 0.1 M phosphate buffer for EM.

Western Blotting—Western blot analysis was performed according to the procedure described in Lee *et al.* (27). LB509 monoclonal anti-α-synuclein antibody was purchased from Zymed Laboratories (South San Francisco, CA).

Immunofluorescence Staining of Cells and Aggregate Fractions—The procedure for cell staining has been described elsewhere (26). Briefly, cells grown on poly-L-lysine-coated coverslips were fixed in 4% paraformaldehyde and permeabilized with 0.1% Triton X-100. Coverslips were then blocked in blocking solution (PBS, 5% bovine serum albumin, 3% goat serum). Primary antibodies in blocking solution were added at dilutions described below and incubated for 30 min: LB509 monoclonal α-synuclein antibody (1:1000, Zymed Laboratories Inc.), 7071 polyclonal α-synuclein antibody (1:1000, provided by Peter Lansbury at Harvard Medical School, Boston, MA), anti-ubiquitin antibody (1:1000, Chemicon), anti-Hsp70/Hsc70 antibody (1:200, StressGen), anti-20S proteasome α-subunit antibody (1:200, Calbiochem-Novabiochem Corp., San Diego, CA). Coverslips were extensively washed for 1–1.5 h with PBS before addition of fluorescent dye (Cy3, Cy2, or Rhodamine Red X)-conjugated goat anti-mouse or anti-rabbit antibodies (1:500, Jackson ImmunoResearch Laboratories, Inc., West Grove, PA) in blocking solution for 30 min. Stainings with Thioflavin S (Sigma) and Hoechst 33258 (Molecular Probes, Inc., Eugene, OR) were performed according to Lee *et al.* (26). For staining of obtained fractions, the samples in PBS were placed on coverslips and let partially dry. After fixing the coverslips in 4% paraformaldehyde in PBS for 30 min, the staining was done in the same manner as described above.

Electron Microscopy—COS-7 cells expressing α-synuclein and α-synuclein fractions in PBS were prepared for section as described in Bouley *et al.* (28). For the immunolabeling, the sections were incubated in 1% gelatin in PBS and then in 0.03 M glycine in PBS. After blocking in 2% bovine serum albumin in PBS, the sections were incubated with LB509 antibody (1:250) in 2% bovine serum albumin in PBS, followed by 10-nm gold-conjugated goat anti-mouse IgG antibody. The sections were stained with 1% uranyl acetate and lead citrate.

For negative staining of fibrils from the inclusion bodies, the pellet from an 80 × *g* spin was rinsed and then resuspended in PBS and incubated in 1% SDS for 20 min at room temperature. After the incubation, the sample was centrifuged at 80 × *g* to remove undissolved inclusion bodies, and the supernatant was centrifuged at 100,000 × *g* for 30 min. The pellet was then resuspended in 50 mM Tris, pH 7.4, and then placed on a carbon-coated grid. The grid was incubated with LB509 antibody (1:250), followed by goat anti-mouse IgG antibody conjugated with a 10-nm gold particle, and after two rinses with distilled water, it was stained with 1% uranyl acetate. The images were obtained using a Philips CM 12 electron microscope.

RESULTS

To characterize the cytoplasmic α-synuclein aggregates, we established a mammalian cell culture model using COS-7 cells and recombinant adenoviral vector. In this model, expression of monomer is saturated at an m.o.i. of about 25, and higher expression over the saturation point induces the spontaneous aggregation, which shows an exponential increase with respect to the increasing m.o.i (40). Alternatively, inhibitors of mitochondrial respiratory chain, such as rotenone, greatly enhance α-synuclein aggregation even at the expression level slightly above the saturation point (m.o.i. of 35), in which the spontaneous aggregation is minimal (26). In this study, the spontaneous α-synuclein aggregation was induced in COS-7 cells at m.o.i. 75, and the resulting cytoplasmic aggregates were characterized using biochemical fractionation combined with imaging analyses.

Similar to what was observed in the rotenone-induced α-synuclein aggregation (26), spontaneous aggregation at m.o.i. 75 resulted in two types of aggregates that are distinct in their sizes and cytoplasmic distributions. One type is represented by small punctate aggregates that are dispersed throughout the cytoplasm, and the other is large juxtanuclear inclusion bodies (Fig. 1). The juxtanuclear inclusion bodies bind to thioflavin S (Fig. 1*B*), a fluorescent dye specific for the highly ordered cross β-sheet structure, thus an indicative of the amyloid-like fibrillar structures (see below for the ultrastructural analysis). In contrast, the small punctate aggregates are thioflavin S-negative (Fig. 1*A*), indicating a non-fibrillar conformation. The difference in the dye binding properties suggests that these two types of aggregates have different structural properties.

Previous immunohistochemical studies of human LBs showed that they are also stained with ubiquitin (29), proteasomes (30), and molecular chaperones, such as hsp70 (11). To determine whether the inclusion bodies in our cell system contain these proteins, we co-stained the cells for α-synuclein with ubiquitin, α-subunit of 20 S proteasome, or hsp70. Like human LBs, large juxtanuclear inclusion bodies were positive for all these proteins (Fig. 1*B*). On the other hand, most of the peripheral punctate aggregates were not stained with ubiquitin, the proteasome subunit, or hsp70 (Fig. 1*A*). Interestingly, the cells with small punctate aggregates display brighter staining in the perinuclear region for ubiquitin, hsp70, and 20 S α-subunit proteins than the cells without aggregates (data not

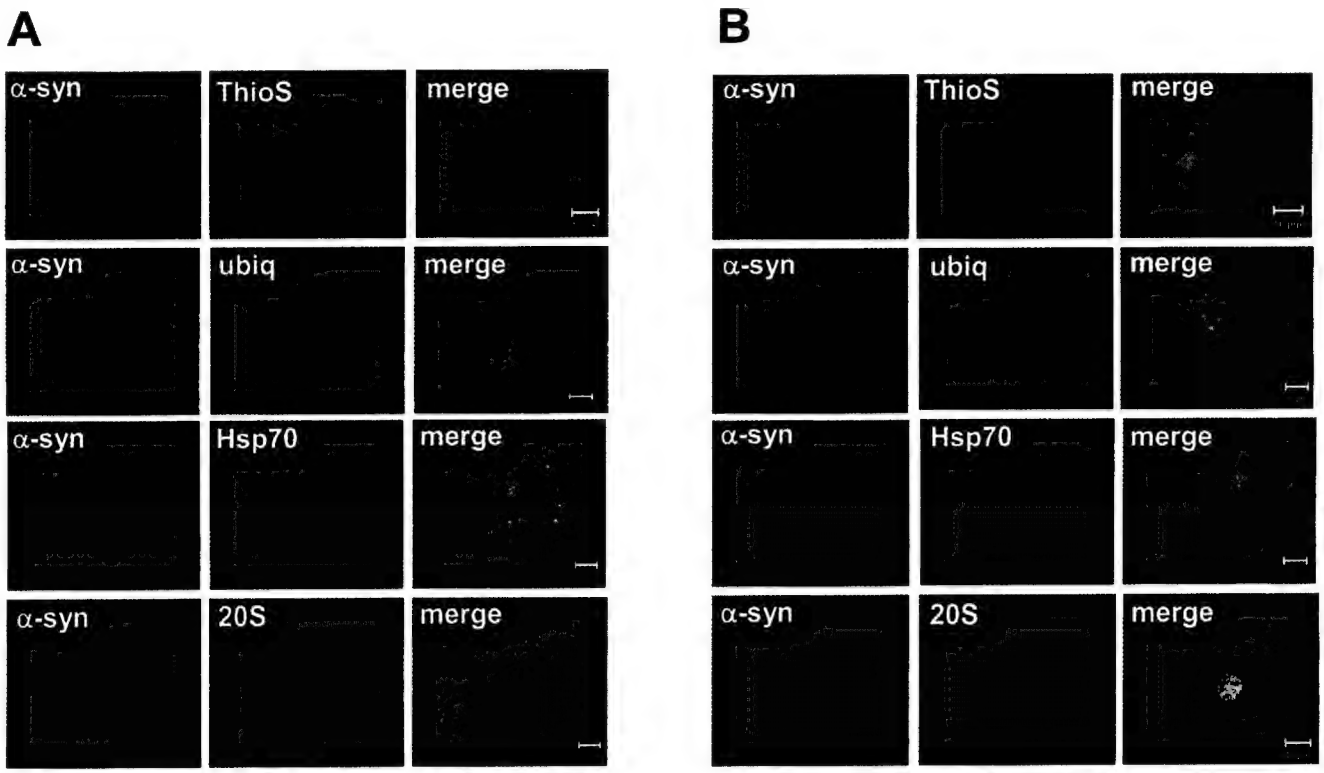

FIG. 1. **Dye-binding property and protein components of the different α-synuclein aggregate species in cells.** α-Synuclein was overexpressed in COS-7 cells by recombinant adenoviral vector at m.o.i. of 75. After 3 days post-infection, α-synuclein aggregates were co-stained with thioflavin S, ubiquitin, hsp70, or 20 S proteasome α-subunit. Small punctate aggregates (*A*) and large juxtanuclear inclusion bodies (*B*) are shown. Note that the small α-synuclein aggregates are thioflavin S-negative and exclude the immunolabels for ubiquitin, hsp70, or 20 S proteasome α-subunit (*A*), whereas inclusion bodies are thioflavin S-positive and contain all these proteins (*B*). Nuclei are stained with Hoechst 33258 (*blue*).

shown), where they show some degree of co-localization with α-synuclein punctate aggregates (Fig. 1*A*). Mitochondria and lysosomes are also elevated and accumulated in the perinuclear region along with the small punctate α-synuclein aggregates (40). The accumulation of these proteins and organelles, which are required for the degradation of macromolecules in the perinuclear region, at what appears to be an early stage of inclusion formation, supports the hypothesis that the inclusion-forming process represents how the cells deliberately sequester and degrade abnormal protein aggregates at the specialized subcellular location.

To further characterize different types of α-synuclein aggregates, we have established a procedure by which these aggregates are separated into different fractions (Fig. 2*A*). Cells that produce α-synuclein aggregates were extracted with 1% Triton X-100 in the culture dish, and the Triton-soluble proteins were gently removed. Under this condition, the soluble monomeric α-synuclein was completely removed, and the aggregates remained in the culture dish, probably due to their association with unknown structures. The remaining Triton-insoluble portion was then scraped in basic pH buffer, in which the aggregates were dissociated from the cellular structures, and centrifuged at 80 × *g*. After the centrifugation at 80 × *g* for 10 min, the pellet fraction was found to contain exclusively the large inclusion bodies, whereas the supernatant contained predominantly small α-synuclein aggregates (see below). In an attempt to further separate the different α-synuclein aggregates, the supernatant was then subjected to a density gradient centrifugation as described in Fig. 2*A*. Western blot analysis of the fractions (fr) identified three distinct fractions containing SDS-resistant α-synuclein aggregates (fr 2, fr 4, and 80 × *g* pellet) (Fig. 2*B*). Although fr 7 also contains α-synuclein aggregates in some cases, immunofluorescence and immuno-EM studies suggested that this fraction consists of clumps of heterogeneous α-synuclein aggregates, which appear to be a mixture of the aggregates found in fr 2 and fr 4 (data not shown).

Dual fluorescence labeling shows that fr 2 and 4 contain small punctate aggregates that are thioflavin S-negative, whereas the 80 × *g* pellet contains large inclusion bodies that are thioflavin S-positive (Fig. 3*A*), confirming the *in situ* immunofluorescence results (Fig. 1). Also consistent with the *in situ* immunofluorescence staining, the small aggregates do not contain ubiquitin, hsp70, or 20 S proteasome α-subunit, whereas the large inclusion bodies in the 80 × *g* pellet were positive for these proteins (Fig. 3, *B–D*). The inclusion bodies were found exclusively in the 80 × *g* pellet. These results confirm that the cells produce different types of α-synuclein aggregates with distinct conformational and compositional properties and that the separation of these aggregates can be achieved using our procedure.

To further analyze the ultrastructural features of α-synuclein aggregates, the fractions were examined by immuno-EM. The aggregates in both fr 2 and fr 4 appear to be non-fibrillar spheres (Fig. 4, *A* and *B*). To compare the size distributions of aggregates in fr 2 and fr 4, we measured the diameter of each aggregate labeled with α-synuclein antibody (Fig. 4*C*). Those aggregates that are irregular in shape were measured across the longest and shortest axes, and the median value was calculated. Random measurement of the diameter of these spheres shows the different size distributions in these fractions, and the calculated mean diameters for fr 2 and fr 4 were 24 and 34 nm, respectively.

EM analysis confirmed that the large inclusion bodies were enriched in the 80 × *g* pellet, and they were immunostained with α-synuclein antibody (Fig. 5*A*). However, in contrast to the small spherical aggregates in fr 2 and fr 4, the inclusions are filled with fibril structures. To further characterize the fibrils of these inclusion bodies, the 80 × *g* pellet was disrupted in 1%

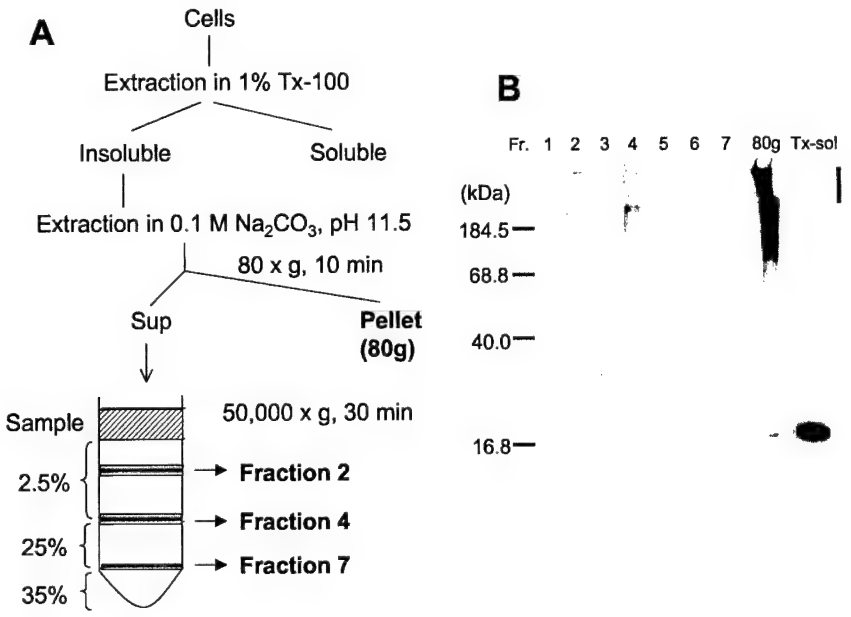

FIG. 2. **Separation of α-synuclein aggregates by density gradient centrifugation.** *A*, schematic diagram of separation procedure. See "Materials and Methods" for details. *B*, Western blotting of the fractions. Note that the fr 2 and fr 4 and the 80 × *g* pellet contain α-synuclein aggregates. The stacking gel portion is indicated as a *line* on the *right side* of the gel.

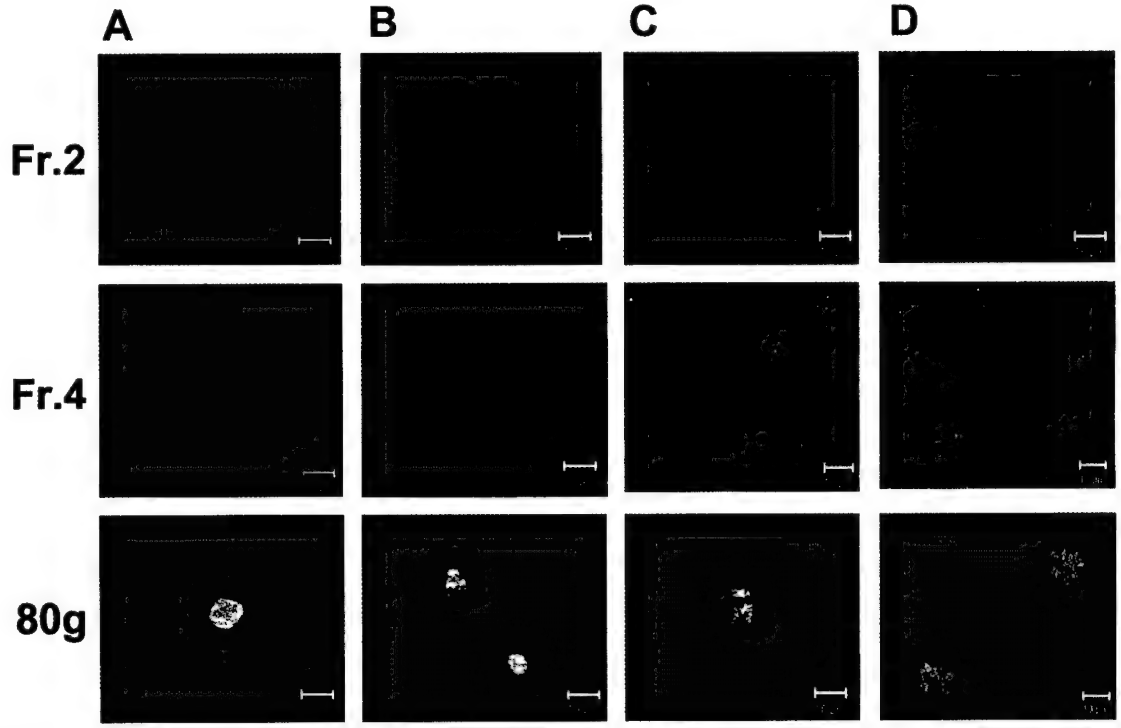

FIG. 3. **Dye-binding properties and protein compositions of fractionated α-synuclein aggregates.** α-Synuclein aggregates in fr 2 and fr 4 and 80 × *g* pellet were co-stained for α-synuclein (*red*) with thioflavin S (*A*, *green*), ubiquitin (*B*, *green*), hsp70 (*C*, *green*), and 20 S proteasome α-subunit (*D*, *green*). Only *merged* images of *red* and *green* are shown. Note that aggregates in fr 2 and fr 4 are thioflavin S-negative and do not contain the proteins tested with a few exceptions, whereas the large inclusion bodies in 80 × *g* pellet are thioflavin S-positive and stained for all the proteins tested here.

SDS, and the released fibrils were collected by 100,000 × *g* centrifugation. The fibrils isolated from the inclusions were 8–13 nm in width and were clearly labeled with α-synuclein antibody (Fig. 5*B*). These fibrils resembled the ones isolated from human LBs (29) or the inclusions of the transgenic mice (12). Thicker structures, which appear to be fibril bundles, were also frequently observed (Fig. 5*C*). These ultrastructural morphologies, along with the thioflavin S binding property, demonstrate that the α-synuclein aggregation process in our cell model produces the inclusion bodies that are composed of α-synuclein fibrils, thus suggesting that this process of inclusion body formation in these cells may resemble the process of LB formation in human brain.

To gain insights into the dynamic relationship between different aggregate species, we investigated the time-dependent formation of the small spherical aggregates and the fibrillar inclusions in the 80 × *g* supernatant and pellet fractions, respectively. As shown in Fig. 6*A*, the small aggregates in the 80 × *g* supernatant became apparent as early as 48 h post-infection and increased with time. On the other hand, the fibrillar inclusions in the 80 × *g* pellet did not appear until 60 h (Fig. 6*A*). This result suggests that the small spherical aggregates are formed before the formation of fibrillar inclusions. We then investigated the time course for the two subspecies of spherical aggregates. Fractionation of the spherical aggregates at different time points shows that the fr 2 aggregates are the

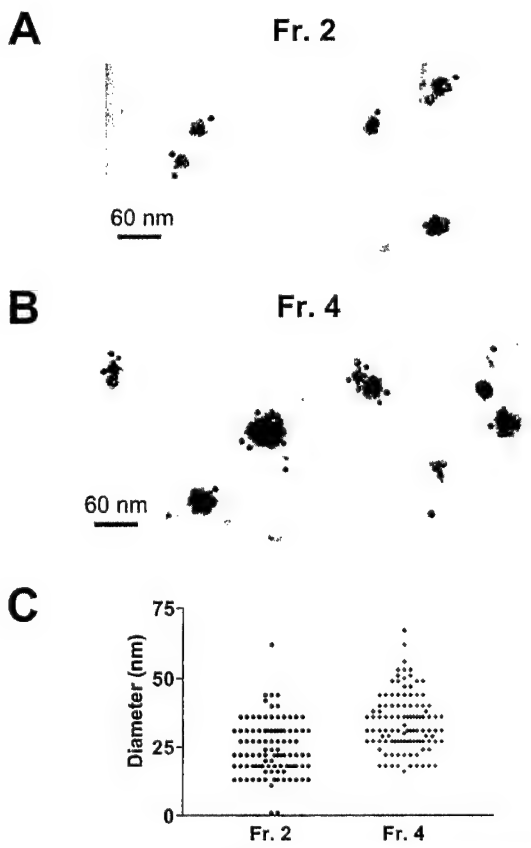

FIG. 4. **Immuno-EM analysis of α-synuclein aggregates from the density gradient fractions.** α-Synuclein aggregates in fr 2 (*A*) and fr 4 (*B*) were labeled with LB509 anti-α-synuclein antibody and 10-nm gold-conjugated secondary antibody. *C*, aggregate size distribution of each gradient fraction. The calculated mean diameters for fr 2 and fr 4 were 24 and 34 nm, respectively.

earliest species formed, appearing at 48 h (Fig. 6*B*, *top panel*). The fr 4 aggregates were formed slightly later at around 54 h (Fig. 6*B*, *second panel*). Both species increased progressively at later time points, but the increase was more dramatic for the fr 4 aggregates (Fig. 6*B*). The fact that these two fractions show differences in both the time of appearance and the rate of increase suggests that they are distinct aggregate species and that the fr 2 aggregates may be the precursors for the fr 4 aggregates.

It has been demonstrated with a number of proteins that the juxtanuclear inclusion formation requires the microtubule-dependent transport of peripheral small aggregates to the pericentriolar region (31, 32). To test whether microtubule-dependent transport is important for the formation of α-synuclein inclusion body, we treated the cells with a microtubule-disrupting agent, nocodazole, and assessed the inclusion formation in two ways. First, the number of inclusion bodies was counted after the immunofluorescence staining (Fig. 7*A*). Second, the relative amounts of inclusion bodies and small non-fibrillar aggregates were measured after the fractionation (Fig. 7*B*). Both analyses clearly show the decrease of the inclusion bodies after nocodazole treatment, implicating the importance of microtubule-dependent transport system in the inclusion formation. Furthermore, the fractionation experiment shows that the reduction of inclusion bodies is accompanied by the increase of the small aggregates (Fig. 7*B*), confirming that nocodazole inhibits the transport of the small aggregates rather than the aggregation *per se*. Interestingly, when the microtubule is disrupted, bigger foci were frequently found in the periphery of the cell (Fig. 7*C*), which implies that the peripheral aggregates can grow bigger to a certain extent, if their transport to the pericentriolar region is blocked. This finding raised a question as to whether the large foci that are grown in the periphery of the cell can acquire the characteristics of the juxtanuclear inclusion bodies. To answer this question, we investigated the thioflavin S binding property and the immunoreactivities for the proteins that are found in the inclusion bodies. Unlike the juxtanuclear inclusion bodies, the large peripheral foci are thioflavin S-negative, indicative of the non-fibrillar nature of the aggregates and devoid of ubiquitin, hsp70, and 20 S proteasome α-subunit (Fig. 7*C*). These data suggest that fibrillation and acquisition of the auxiliary proteins are not spontaneous consequences of the aggregate growth, rather, they are closely linked to the microtubule-dependent inclusion-forming process.

DISCUSSION

In our previous study, we have demonstrated that overexpression of α-synuclein or exposure of cells to mitochondrial inhibitors produces two distinct forms of α-synuclein aggregate; small punctate aggregates that are scattered throughout the cytoplasm and large juxtanuclear inclusion bodies. Here, we have characterized the structural natures of these aggregates and investigated the relationship between them in the context of inclusion forming process. Using biochemical fractionation and EM analysis, we have demonstrated small aggregates are non-fibrillar spheres, and the inclusion bodies are filled with α-synuclein fibrils. Time-dependent analysis shows that small non-fibrillar aggregates precede the formation of fibrillar inclusions. An anti-microtubule agent, nocodazole, causes a reduction in the number of fibrillar inclusions and the accumulation of non-fibrillar aggregates in the cytoplasm, suggesting that these non-fibrillar aggregates are the precursors of the fibrillar aggregates in the inclusion bodies. Protofibrils are described as non-fibrillar aggregates that precede the fibril formation and are often enriched with β-sheet structure (20). Although the conformational characteristics of the cytoplasmic aggregates are not yet available, the ultrastructural and kinetic properties suggest that the small non-fibrillar aggregates are the cellular equivalents of the protofibrils.

In solution, fibrillation of α-synuclein, which involves a number of metastable intermediate species, including various protofibrils, is a continuous process, because all the monomers and assembly intermediates are freely diffusible and available for the molecular interactions. However, in cells, fibrillar α-synuclein aggregates are found exclusively in the juxtanuclear inclusions, and interfering with the transport of protofibrils to the pericentriolar region inhibits the fibril formation. These findings support the hypothesis that monomer to protofibril conversion and protofibril to fibril conversion are spatially separate processes; the former seems to be a diffusion-limited reaction that occurs throughout the cytoplasm, whereas the latter is restricted only in the pericentriolar region. In cells, the protofibrils seem to be associated with detergent-insoluble structures,[2] which limits their chance to interact with one another. When microtubule-mediated transport is disrupted with nocodazole, peripheral protofibrils become larger than normal but do not turn into fibrils. Thus, it is only after the protofibrils are transported and deposited in the pericentriolar region that the interactions between the protofibrils are allowed to undergo the transformation into fibrils.

Protofibrillar intermediates (often in a spherical morphology) have been found in virtually all fibrillation characterized, thus becoming a universal mechanism of amyloid-like fibril formation (33–36). However, the mechanism of the protofibril-

[2] H.-J. Lee and S.-J. Lee, unpublished data.

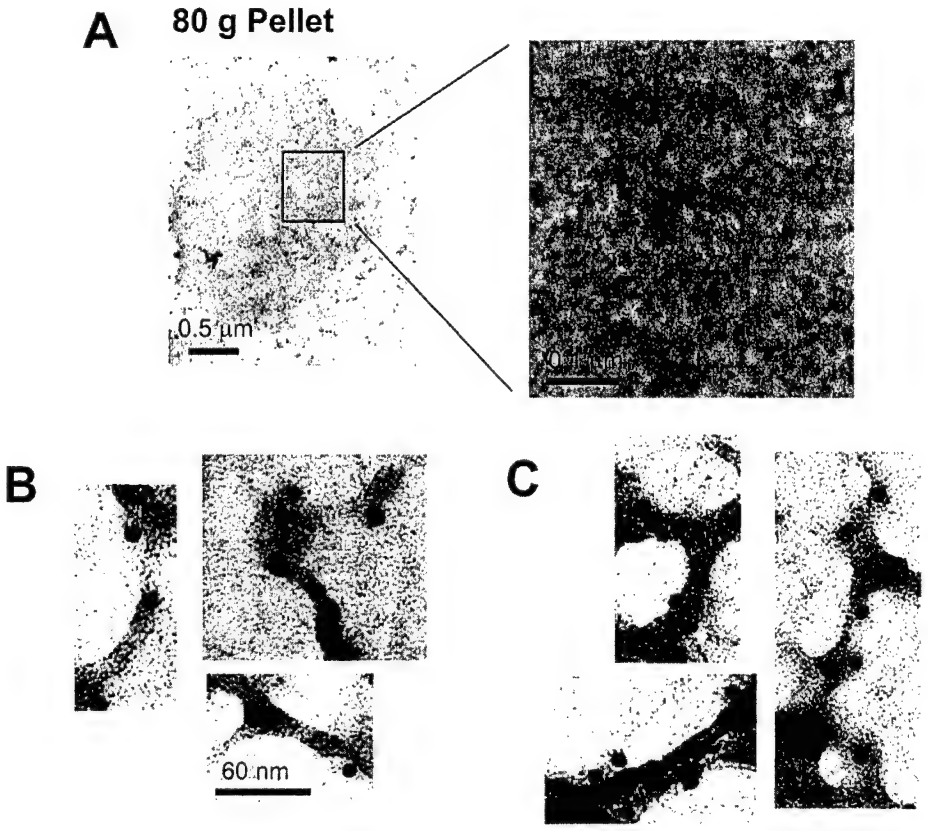

FIG. 5. **Ultrastructural analysis of α-synuclein inclusion bodies in the 80 × *g* pellet.** *A*, inclusion bodies in the 80 × *g* pellet were labeled with LB509 and 10-nm gold-conjugated secondary antibody. A high magnification image of the *boxed region* on the *left image* is shown on the *right*. Note the fibril-like structures on the magnified image. *B* and *C*, immuno-EM images of individual fibrils (*B*) and fibril bundles (*C*). The α-synuclein inclusion bodies in the 80 × *g* pellet were disrupted with 1% SDS, and the released fibrils were labeled with LB509, followed by the staining with uranyl acetate.

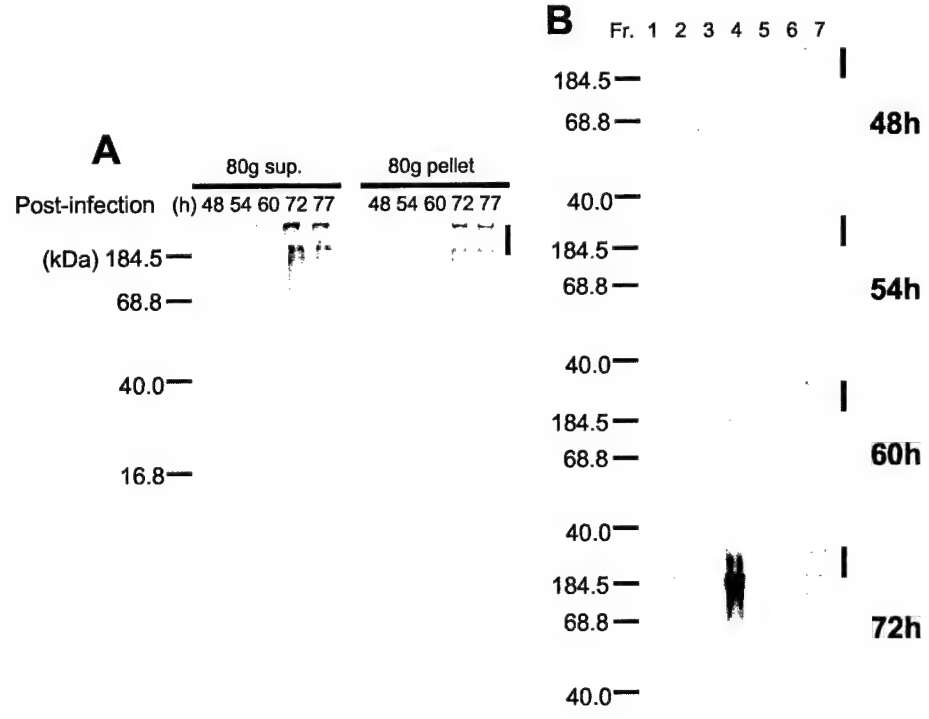

FIG. 6. **Time-dependent progression of α-synuclein aggregates.** *A*, non-fibrillar α-synuclein aggregates and inclusion bodies were obtained in the 80 × *g* supernatant and the pellet, respectively, at times indicated, and analyzed with LB509 antibody. *B*, subspecies of non-fibrillar α-synuclein aggregates in the 80 × *g* supernatant was further fractionated at times indicated. The stacking gel portion is indicated as a *line* on the *right side* of the gel.

to-fibril transition is not clearly understood. *In vitro*, most α-synuclein protofibrils are either in a spherical shape or in the morphologies (chain-like and annular pore-like structures) that appear to be produced by the association of the spherical protofibrils (20, 21). This observation implies that the protofibril spheres can self-associate to form higher-order structures. A similar mechanism has been proposed in the fibrillation of sup35 protein (N-terminal and mid-domain fragment) in which oligomer-oligomer interactions precede the conformational changes to amyloid-like fibrils (34). Our observation that the fibril formation occurs only when the protofibrils are concentrated and allowed to interact with one another also supports the possibility that the fibril formation *in vivo* could be driven by protofibril-protofibril interactions. However, our findings do not exclude the role of monomers in the cellular fibrillation process. Direct incorporation of monomers into the fibrils could also play a role in fibril growth *in vivo*. *In vitro* studies show that when the protofibrils are populated in solution, the transition from spherical aggregates to the amyloid-like fibrils is a spontaneous process. However, in cells this process may be

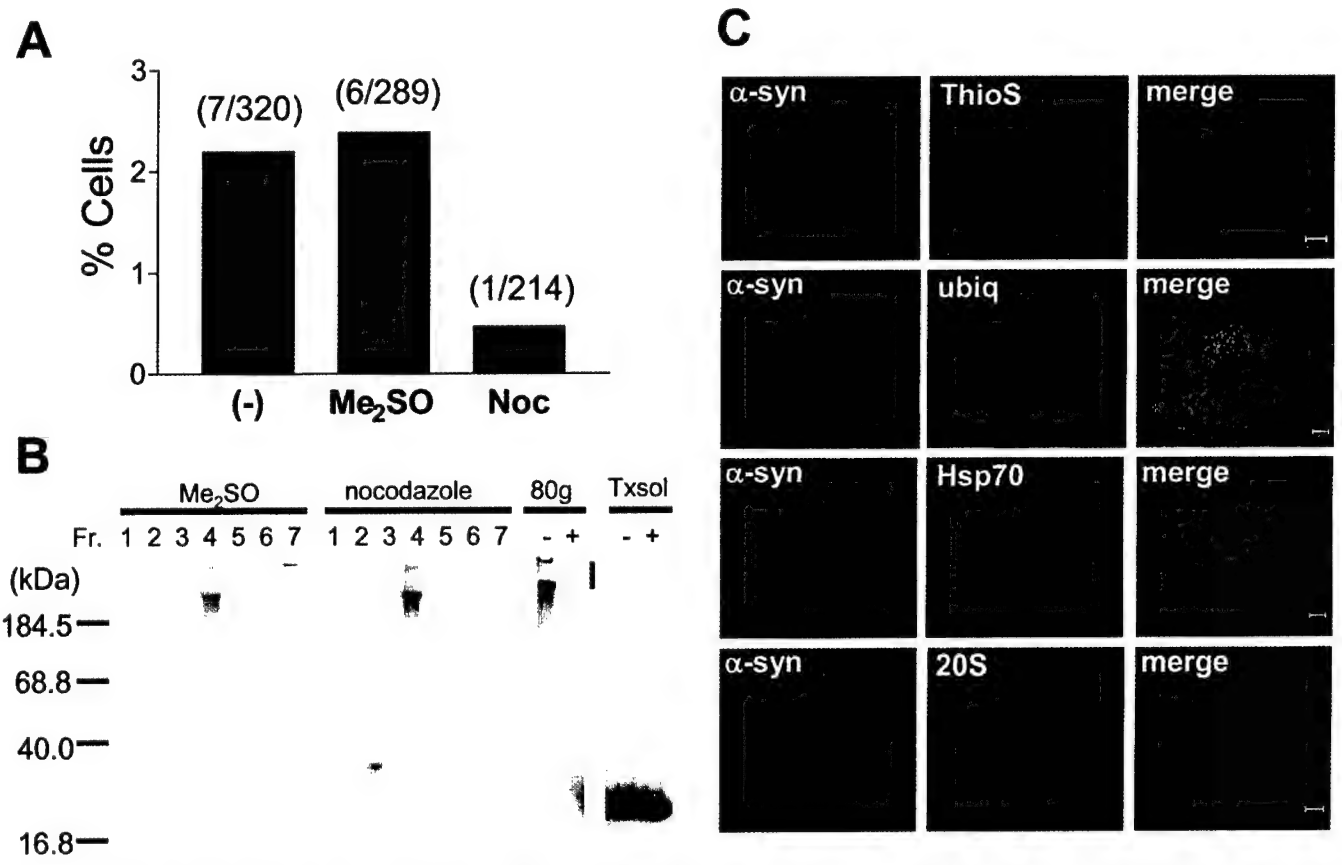

FIG. 7. **Nocodazole treatment inhibits the progression of peripheral α-synuclein aggregates into juxtanuclear fibrillar inclusions.** *A*, percentage of cells with inclusion bodies. COS-7 cells overexpressing α-synuclein were treated with Me_2SO or nocodazole (10 μg/ml) for 48 h before the immunofluorescence labeling for α-synuclein and counting. The *numbers* above each *bar* indicate the number of cells with inclusion bodies per the total number of cells counted. For each sample, ten random fields were selected for counting. *B*, reduction in inclusion bodies and concomitant increase of small non-fibrillar aggregates after the nocodazole treatment. COS-7 cells expressing α-synuclein were treated with Me_2SO or nocodazole for 24 h before extraction, and the aggregates were fractionated according to the procedure described in Fig. 2. The fractions were analyzed by Western blotting with LB509 antibody. The stacking gel portion is indicated as a *line* on the *right side* of the gel. *Txsol*, Triton X-100-soluble fraction; −, dimethyl sulfoxide (*Me_2SO*); +, nocodazole. *C*, enlarged peripheral α-synuclein aggregates were found in the cells that were treated with nocodazole. These enlarged peripheral foci did not stain with thioflavin S or the antibodies against ubiquitin, hsp70, or 20 S proteasome α-subunit.

assisted by the proteins that are co-accumulated with α-synuclein aggregates in the pericentriolar region, such as molecular chaperones.

Microtubule-dependent deposition of peripheral aggregates into the pericentriolar region has been documented with several other proteins, and the resulting inclusion bodies are referred to as aggresomes (37, 38). Aggresome represents one of the end points of cellular responses to misfolded proteins, with other competing end points being degradation and refolding. Although many proteins share the same mechanism for the deposition in the pericentriolar region, the physical states of the final aggregated forms seem to be determined by the conformational properties of individual proteins. For example, aggregates of cystic fibrosis transmembrane conductance regulator (31) or GFP-250 (32) remain granular in shape, whereas α-synuclein aggregates are transformed into fibrils after deposition in the aggresomes. If the recent proposal is correct that protofibrils are the pathogenic species (20), accelerating the transformation of disease-associated protofibrils into fibrils would have evolutionary advantage. Developing noninvasive ways to interfere with the transport of protofibrils to the inclusion-forming site or the structural transition to fibrils will allow us to assess the role of these processes in α-synuclein-mediated cell death.

Inclusion bodies, either the ones that are produced in our cell system or LBs in human brain, contain protein components other than α-synuclein fibrils, such as proteasome subunits (30), ubiquitin (29), and molecular chaperones (11). Their presence in inclusion bodies raises the question of whether they co-aggregate with α-synuclein or even promote the aggregation process. Our study shows that α-synuclein protofibrils, both the ones in the cells or isolated from the cells, are not stained for these proteins, but they are co-deposited in the perikaryal region with α-synuclein protofibrils. In a previous study, we have shown that early stage α-synuclein oligomerization in crude cytosol preparation is highly self-selective (19). In agreement with our findings, Rajan *et al.* (39) have recently demonstrated that aggregation of misfolded proteins is the result of highly specific self-association, rather than nonspecific interactions between unrelated proteins. Therefore, it is unlikely that the proteins that co-exist in the inclusion bodies play a direct role in promoting α-synuclein aggregation. Rather, it seems more likely that the presence of protein degradation machineries and the molecular chaperones is an indication of an attempt by the cell to clear these protein deposits.

Fractionation of protofibrillar aggregates resulted in the separation of two subspecies with distinct size distribution. It is not entirely clear at the moment whether they represent two distinct intermediates in a linear process or one of them is an artificial outcome that are formed during the extraction procedure, such as fragmentation of larger aggregates to smaller pieces or large clumps of aggregates due to an incomplete resuspension. If they were the same species, it would be predicted that their kinetic behavior is identical. However, our

time-course experiment shows that these two species have clearly distinctive kinetics: the smaller species appears first, followed by the larger one. Thus, it is likely that they are distinct entities and may be related in a linear process.

In conclusion, we have demonstrated that α-synuclein fibrillation is tightly associated with the microtubule-dependent inclusion-forming process, which seems to be necessary for the protofibril-to-fibril transition. The ability to separate different species and semi-quantitatively analyze them will allow the detailed characterization of the α-synuclein aggregation process in cells.

Acknowledgments—We thank P. Lansbury for reading the manuscript, H. Lashuel for his critical comments, S. Patel for technical assistance, and N. Ghori for the assistance for EM analysis.

REFERENCES

1. Trojanowski, J. Q., Goedert, M., Iwatsubo, T., and Lee, V. M. (1998) *Cell Death Differ.* **5,** 832–837
2. Goedert, M. (2001) *Nat. Rev. Neurosci.* **2,** 492–501
3. Polymeropoulos, M. H., Lavedan, C., Leroy, E., Ide, S. E., Dehejia, A., Dutra, A., Pike, B., Root, H., Rubenstein, J., Boyer, R., Stenroos, E. S., Chandrasekharappa, S., Athanassiadou, A., Papapetropoulos, T., Johnson, W. G., Lazzarini, A. M., Duvoisin, R. C., Di Iorio, G., Golbe, L. I., and Nussbaum, R. L. (1997) *Science* **276,** 2045–2047
4. Kruger, R., Kuhn, W., Muller, T., Woitalla, D., Graeber, M., Kosel, S., Przuntek, H., Epplen, J. T., Schols, L., and Riess, O. (1998) *Nat. Genet.* **18,** 106–108
5. Conway, K. A., Harper, J. D., and Lansbury, P. T. (1998) *Nat. Med.* **4,** 1318–1320
6. Narhi, L., Wood, S. J., Steavenson, S., Jiang, Y., Wu, G. M., Anafi, D., Kaufman, S. A., Martin, F., Sitney, K., Denis, P., Louis, J. C., Wypych, J., Biere, A. L., and Citron, M. (1999) *J. Biol. Chem.* **274,** 9843–9846
7. Li, J., Uversky, V. N., and Fink, A. L. (2001) *Biochemistry* **40,** 11604–11613
8. Conway, K. A., Lee, S.-J., Rochet, J. C., Ding, T. T., Williamson, R. E., and Lansbury, P. T., Jr. (2000) *Proc. Natl. Acad. Sci. U. S. A.* **97,** 571–576
9. Feany, M. B., and Bender, W. W. (2000) *Nature* **404,** 394–398
10. Masliah, E., Rockenstein, E., Veinbergs, I., Mallory, M., Hashimoto, M., Takeda, A., Sagara, Y., Sisk, A., and Mucke, L. (2000) *Science* **287,** 1265–1269
11. Auluck, P. K., Chan, H. Y., Trojanowski, J. Q., Lee, V. M., and Bonini, N. M. (2002) *Science* **295,** 865–868
12. Giasson, B. I., Duda, J. E., Quinn, S. M., Zhang, B., Trojanowski, J. Q., and Lee, V. M.-Y. (2002) *Neuron* **34,** 521–533
13. Lee, M. K., Stirling, W., Xu, Y., Xu, X., Qui, D., Mandir, A. S., Dawson, T. M., Copeland, N. G., Jenkins, N. A., and Price, D. L. (2002) *Proc. Natl. Acad. Sci. U. S. A.* **99,** 8968–8973
14. Betarbet, R., Sherer, T. B., MacKenzie, G., Garcia-Osuna, M., Panov, A. V., and Greenamyre, J. T. (2000) *Nat. Neurosci.* **3,** 1301–1306
15. Weinreb, P. H., Zhen, W., Poon, A. W., Conway, K. A., and Lansbury, P. T., Jr. (1996) *Biochemistry* **35,** 13709–13715
16. Eliezer, D., Kutluay, E., Bussell, R., Jr., and Browne, G. (2001) *J. Mol. Biol.* **307,** 1061–1073
17. Wood, S. J., Wypych, J., Steavenson, S., Louis, J. C., Citron, M., and Biere, A. L. (1999) *J. Biol. Chem.* **274,** 19509–19512
18. Uversky, V. N., Li, J., and Fink, A. L. (2001) *J. Biol. Chem.* **276,** 10737–10744
19. Uversky, V. N., Lee, H.-J., Li, J., Fink, A. L., and Lee, S.-J. (2001) *J. Biol. Chem.* **276,** 43495–43498
20. Goldberg, M. S., and Lansbury, P. T., Jr. (2000) *Nat. Cell Biol.* **2,** E115–E119
21. Ding, T. T., Lee, S.-J., Rochet, J. C., and Lansbury, P. T. (2002) *Biochemistry* **41,** 10209–10217
22. Conway, K. A., Harper, J. D., and Lansbury, P. T., Jr. (2000) *Biochemistry* **39,** 2552–2563
23. Volles, M. J., Lee, S.-J., Rochet, J. C., Shtilerman, M. D., Ding, T. T., Kessler, J. C., and Lansbury, P. T., Jr. (2001) *Biochemistry* **40,** 7812–7819
24. Volles, M. J., and Lansbury, P. T., Jr. (2002) *Biochemistry* **41,** 4595–4602
25. Lashuel, H. A., Hartley, D., Petre, B. M., Walz, T., and Lansbury, P. T. (2002) *Nature* **418,** 291
26. Lee, H.-J., Shin, S. Y., Choi, C., Lee, Y. H., and Lee, S.-J. (2002) *J. Biol. Chem.* **277,** 5411–5417
27. Lee, S.-J., Liyanage, U., Bickel, P. E., Xia, W., Lansbury, P. T., Jr., and Kosik, K. S. (1998) *Nat. Med.* **4,** 730–734
28. Bouley, D. M., Ghori, N., Mercer, K. L., Falkow, S., and Ramakrishnan, L. (2001) *Infect. Immun.* **69,** 7820–7831
29. Spillantini, M. G., Crowther, R. A., Jakes, R., Hasegawa, M., and Goedert, M. (1998) *Proc. Natl. Acad. Sci. U. S. A.* **95,** 6469–6473
30. Ii, K., Ito, H., Tanaka, K., and Hirano, A. (1997) *J. Neuropathol. Exp. Neurol.* **56,** 125–131
31. Johnston, J. A., Ward, C. L., and Kopito, R. R. (1998) *J. Cell Biol.* **143,** 1883–1898
32. Garcia-Mata, R., Bebok, Z., Sorscher, E. J., and Sztul, E. S. (1999) *J. Cell Biol.* **146,** 1239–1254
33. Bucciantini, M., Giannoni, E., Chiti, F., Baroni, F., Formigli, L., Zurdo, J., Taddei, N., Ramponi, G., Dobson, C. M., and Stefani, M. (2002) *Nature* **416,** 507–511
34. Serio, T. R., Cashikar, A. G., Kowal, A. S., Sawicki, G. J., Moslehi, J. J., Serpell, L., Arnsdorf, M. F., and Lindquist, S. L. (2000) *Science* **289,** 1317–1321
35. Harper, J. D., Wong, S. S., Lieber, C. M., and Lansbury, P. T., Jr. (1999) *Biochemistry* **38,** 8972–8980
36. Poirier, M. A., Li, H., Macosko, J., Cai, S., Amzel, M., and Ross, C. A. (2002) *J. Biol. Chem.* **277,** 41032–41037
37. Kopito, R. R. (2000) *Trends Cell Biol.* **10,** 524–530
38. Garcia-Mata, R., Gao, Y. S., and Sztul, E. (2002) *Traffic* **3,** 388–396
39. Rajan, R. S., Illing, M. E., Bence, N. F., and Kopito, R. R. (2001) *Proc. Natl. Acad. Sci. U. S. A.* **98,** 13060–13065
40. Gosavi, N., Lee, H.-J., Lee, J. S., Patel, S., and Lee, S.-J. (2002) *J. Biol. Chem.* **277,** 48984–48992

THE JOURNAL OF BIOLOGICAL CHEMISTRY Vol. 277, No. 50, Issue of December 13, pp. 48984–48992, 2002

Printed in U.S.A.

Golgi Fragmentation Occurs in the Cells with Prefibrillar α-Synuclein Aggregates and Precedes the Formation of Fibrillar Inclusion*

Received for publication, August 9, 2002, and in revised form, September 10, 2002
Published, JBC Papers in Press, September 25, 2002, DOI 10.1074/jbc.M208194200

Nirmal Gosavi, He-Jin Lee, Jun Sung Lee‡, Smita Patel, and Seung-Jae Lee§

From The Parkinson's Institute, Sunnyvale, California 94089

Amyloid-like fibrillar aggregates of intracellular proteins are common pathological features of human neurodegenerative diseases. However, the nature of pathogenic aggregates and the biological consequences of their formation remain elusive. Here, we describe (i) a model cellular system in which prefibrillar α-synuclein aggregates and fibrillar inclusions are naturally formed in the cytoplasm with distinctive kinetics and (ii) a tight correlation between the presence of prefibrillar aggregates and the Golgi fragmentation. Consistent with the structural abnormality of Golgi apparatus, trafficking and maturation of dopamine transporter through the biosynthetic pathway were impaired in the presence of α-synuclein aggregates. Reduction in cell viability was also observed in the prefibrillar aggregate-forming condition and before the inclusion formation. The fibrillar inclusions, on the other hand, showed no correlation with Golgi fragmentation and were preceded by these events. Furthermore, at the early stage of inclusion formation, active lysosomes and mitochondria were enriched in the juxtanuclear area and co-aggregate into a compact inclusion body, suggesting that the fibrillar inclusions might be the consequence of an attempt of the cell to remove abnormal protein aggregates and damaged organelles. These results support the hypothesis that prefibrillar α-synuclein aggregates are the pathogenic species and suggest that Golgi fragmentation and subsequent trafficking impairment are the specific consequence of α-synuclein aggregation.

Many human neurological disorders, including Parkinson's disease, dementia with Lewy bodies, and multiple system atrophy, are characterized by amyloid-like fibrillar aggregates of α-synuclein, such as Lewy bodies (LBs)[1] and Lewy neurites (1, 2). α-Synuclein is a 140-amino acid protein that is enriched in presynaptic terminals of neurons (3). In the test tube, this protein forms fibrils, which resemble the ones isolated from postmortem brains with LB diseases (4–6). A causative role of fibrillar α-synuclein inclusions in neurodegeneration has been suggested in a mouse model in which formation of intracytoplasmic α-synuclein inclusions coincided with the severe motor impairment (7). On the other hand, a study in a transgenic fly model that express human α-synuclein has shown that co-expression of molecular chaperone hsp70 alleviated the neurodegenerative phenotype but did not reduce the formation of α-synuclein-positive inclusion bodies (8). This result raised a question as to whether the fibrillar inclusions play a causative role in neurodegenerative process. Furthermore, recent *in vitro* studies revealed various non-fibrillar species during the course of fibrillation and suggested a possibility that these metastable intermediate species, not the fibrils themselves, might elicit cytotoxicity (9, 10). Elucidating which particular aggregate species possess the principal cytotoxic effect holds the key to understanding the etiologic role of protein aggregation in the disease pathogenesis. Study of this problem, however, has been hampered by the lack of an experimental system in which intermediates of the endogenous fibrillation process can be biochemically defined and analyzed. Here, we have established such a system and have assessed the effects of prefibrillar intermediates that are formed naturally in the cytoplasm. In this report, we refer to prefibrillar aggregates as non-fibrillar oligomeric assemblies that precede the formation of fibrils and to inclusions as large deposits of aggregates that are usually found in juxtanuclear location.

MATERIALS AND METHODS

Antibodies—Monoclonal anti-α-synuclein antibody, LB509, was purchased from Zymed Laboratories (South San Francisco, CA), and a polyclonal anti-α-synuclein serum, 7071, was provided by Peter Lansbury (Brigham and Women's Hospital, Boston, MA). Antibodies against GM130, TGN46, and calnexin were obtained from BD Biosciences (San Diego, CA), Serotec (Oxford, UK), and StressGen Biotechnologies Corp. (Victoria, BC, Canada), respectively. Antibodies for mannosidase II and DAT were purchased from Chemicon (Temecula, CA). All the fluorescently labeled secondary antibodies were purchased from Jackson ImmunoResearch Laboratories (West Grove, PA). ^{125}I-Labeled anti-mouse IgG antibody was obtained from Amersham Biosciences (Piscataway, NJ). Goat anti-mouse IgG antibody, conjugated with a 10-nm gold particle, was obtained from Ted Pella Inc. (Redding, CA).

Aggregation Analysis at Different Multiplicity of Infection—Different amounts (see Fig. 1 legend) of adeno/α-syn (11) and empty viral vector were mixed to make the final number of viral particle be 1.5×10^8. COS-7 cells (1.5×10^6 cells) were infected with these mixtures as described previously (11). At day 3, the cells were extracted in phosphate-buffered saline (PBS) with 1% Triton X-100 and protease inhibitor mixture (Sigma), and the extracts were centrifuged at 16,000 × *g* for 5 min to separate detergent-soluble (supernatant) and insoluble (pellet) fractions. The pellets were resuspended in half the volume of 1× Laemmli sample buffer. Ten micrograms of supernatant and the equal

* This work was supported in part by the U. S. Army Medical Research Acquisition Activity (DAMD17-02-0171) the Abramson Family Foundation, and a visiting fellowship from BK21 project, Ministry of Education, Republic of Korea (to J. S. L.). The costs of publication of this article were defrayed in part by the payment of page charges. This article must therefore be hereby marked "*advertisement*" in accordance with 18 U.S.C. Section 1734 solely to indicate this fact.

‡ Present address: Division of Molecular and Life Science, Pohang University of Science and Technology, Pohang 790-784, Republic of Korea.

§ To whom correspondence should be addressed: The Parkinson's Institute, 1170 Morse Ave., Sunnyvale, CA 94089. Tel.: 408-542-5642; Fax: 408-734-8522; E-mail: slee@thepi.org.

[1] The abbreviations used are: LB, Lewy body; PBS, phosphate-buffered saline; m.o.i., multiplicity of infection; EM, electron microscopy; BSA, bovine serum albumin; GA, Golgi apparatus; AD, Alzheimer's disease; ALS, amyotrophic lateral sclerosis; CJD, Creutzfeldt-Jakob disease; MSA, multiple system atrophy; DAT, dopamine transporter; endoH, endoglycosidase H; ER, endoplasmic reticulum.

volume of pellet were applied onto 12% SDS-polyacrylamide gel and subjected to Western blotting (12). For the quantitative analysis, the proteins were visualized using ^{125}I-labeled secondary antibody, and the monomers and the aggregate smears (from 60 kDa to the top of the gel) were quantified by computer-assisted densitometry using ImageQuaNT software (Molecular Dynamics) under equal light and power settings. Three independent experiments were performed.

For the Golgi analysis and cell viability assay, the cells were split onto cover-glasses into 12-well plates and into 35-mm dishes, respectively, at day 1 (the next day of infection) and incubated until the time of analysis, usually at day 3 or 4. We have noticed that the time course of the aggregation process changes slightly depending on the surface area of the tissue culture dish; *i.e.* aggregation is faster in 100-mm dishes than in 35-mm dishes. To normalize the effects of viral vector itself, the total amount of viral particles was adjusted to be equivalent with empty viral vector in all experiments.

Extraction and Separation of Prefibrillar Aggregates and Fibrillar Inclusions—COS-7 cells were infected with adeno/α-syn at m.o.i. 75, and the cells were split into 35-mm dishes at day 1 and incubated until days 3 or 4. On the day of extraction, buffer T (0.25 M sucrose, 25 mM KCl, 5 mM $MgCl_2$, 20 mM Tris, pH 7.5, 1% Triton X-100, protease inhibitor mixture) was added gently onto each dish and incubated at room temperature for 5 min. The Triton X-soluble supernatant was removed carefully and then buffer N (0.1 M Na_2CO_3, pH 11.5, with 1% Triton X-100 and protease inhibitor mixture) was added to each dish, and extract was obtained by scraping dishes and repeated pipetting. After incubation on ice for 5 min, the extract was centrifuged at 80 × *g* for 5 min, at which condition only the fibrillar inclusions sedimented to form a pellet (43). The prefibrillar aggregates in the supernatant were collected by additional centrifugation at 16,000 × *g* for 10 min.

Fluorescence Microscopy—Fluorescence staining, including nuclear staining with Hoechst 33258, was performed according to the procedures in Lee *et al.* (11). For the staining of lysosomes and mitochondria, the cells were incubated with 100 nM Lysotracker (Molecular Probes) and 200 nM Mitotracker (Molecular Probes), respectively, in the growth medium for 30 min, and then fixed and permeabilized. Morphology of GA was visualized using an antibody against GM130, TGN46, or mannosidase II. All the fluorescence images in this study were obtained with a laser scanning confocal microscope (LSM PASCAL, Zeiss). For quantitative analysis, images were obtained by the "tile-scan" of area of 0.48 mm^2, and the number of cells with fragmented Golgi (Fig. 3) or fibrillar inclusions (Fig. 2) was counted in three random areas. Each image contained 140 cells on average, and the experiment was repeated more than three times. Golgi fragmentation was defined as the dispersion of small Golgi-immunoreactive foci. Only the cells with completely scattered Golgi fragments were counted, whereas the cells with long tubular Golgi staining were not. Thus, the percentage obtained in this study is likely to under-represent the actual degree of Golgi fragmentation.

Electron Microscopy—For electron microscopy (EM), α-synuclein was expressed in COS-7 cells at m.o.i. 75 for 4 days. The sections were prepared as described in Bouley *et al.* (13). Briefly, the cells were fixed in 2% glutaraldehyde in 0.1 M phosphate buffer, pH 7.2, on ice for 35 min. After the post-fix in 1% osmium tetroxide at room temperature for 30 min, the cells were stained with 1% uranyl acetate for 1 h and then dehydrated with a series of different concentrations of ethanol. After the samples were embedded in gelatin capsule, the sections were prepared on carbon-coated nickel grids and stained with 1% uranyl acetate. For the immunolabeling, the sections were incubated in 1% gelatin/PBS, followed by 0.03 M glycine/PBS. After a rinse with 2% bovine serum albumin (BSA)/PBS, the sections were incubated with LB509 antibody (1/250 dilution) in 2% BSA/PBS, and then with 10-nm gold-conjugated goat anti-mouse IgG antibody. The sections were then stained with 1% uranyl acetate and lead citrate and observed with a Philips CM 12 electron microscope.

Biotinylation and Isolation of Cell Surface Proteins—Cells were infected with various ratios of α-synuclein and empty viral vectors as described before and incubated until day 3. For the expression of dopamine transporter (DAT), the infected cells were transfected with hDAT/pCDNA3.1(+) on the next day. Biotinylation and isolation of cell surface proteins were carried out according to Melikian *et al.* (14), and all the procedures were performed on ice except where indicated otherwise. Briefly, the cells were rinsed twice with PBS^{2+} (PBS with 0.1 mM $CaCl_2$ and 1.0 mM $MgCl_2$) and incubated with 1.0 mg/ml NHS-SS-biotin (Pierce, Rockford, IL) in PBS^{2+} for 20 min twice. Remaining reactive NHS-SS-biotin was quenched twice with 0.1 M glycine for 20 min, and then the cells were extracted in radioimmune precipitation assay buffer (10 mM Tris, pH 7.4, 150 mM NaCl, 1.0 mM EDTA, 0.1% SDS, 1% Triton X-100, 0.5% sodium deoxycholate, protease inhibitor mixture (Sigma)). The cell extracts with the same amounts of protein were incubated with Immunopure streptavidin beads (Pierce) at room temperature for 45 min with constant rotation. The bound fractions were washed four times with radioimmune precipitation assay buffer and eluted with 1× Laemmli sample buffer. The unbound fractions were precipitated with 5% trichloroacetic acid and dissolved in 1× Laemmli sample buffer. The samples were loaded onto SDS-PAGE and analyzed by Western blotting. Due to the abundance of cytoplasmic DAT relative to the cell surface DAT, one-hundredth equivalents of unbound samples (cytoplasmic proteins) were loaded.

Cell Viability Assay—The cells were trypsinized, and one-tenth of cells were mixed with the equal volume of 0.4% trypan blue solution (Sigma). The number of cells that exclude the dye was counted using a hemacytometer in triplicate. The data in Fig. 10 were obtained from two independent experiments. The rest of the trypsinized cells were extracted and fractionated as described above, and the detergent-insoluble fractions were subjected to Western blotting with LB509 antibody.

RESULTS

Prefibrillar α-Synuclein Aggregates in the Cytoplasm—To characterize the aggregation process of α-synuclein in cells, we introduced various amounts of the cDNA into COS-7 cells using recombinant adenoviral vector (adeno/α-syn) and quantitatively analyzed the changes in the amounts of the monomers and aggregates. The level of monomers increased linearly with the increase of multiplicity of infection (m.o.i.) before reaching a plateau (~1.7% of total cellular protein). Once the monomer level reached the plateau, the levels of aggregates elevated in response to increased m.o.i. (Fig. 1*A*). This non-linear relationship between the monomer level and the aggregation allows us to selectively investigate the effects of the monomers or aggregates by choosing the appropriate m.o.i. range. Two different types of α-synuclein aggregates were found by immunofluorescence staining: small punctate aggregates that are dispersed throughout the cytoplasm and large juxtanuclear inclusion bodies (43). The large inclusions were strongly stained with thioflavin S, a fluorescent dye specific to amyloid-like structure, whereas the small punctate aggregates were not (43). Electron microscopy (EM) shows that the inclusion bodies are filled with filaments with the width of 8–10 nm, and they were labeled with α-synuclein antibody (Fig. 1*C*). The presence of α-synuclein fibrils in the inclusions was further confirmed by immunogold labeling of individual fibrils that were isolated from the inclusion preparations. Immuno-EM study also verified the non-fibrillar nature of small punctate aggregates upon isolation using the procedure described below (43).

A small amount of aggregates appeared at day 2 post-infection and increased drastically at day 3 with a small further increase at day 4, whereas the monomer levels remained constant throughout this period (Fig. 2*A*). Until day 3, most of the aggregates were small, non-fibrillar ones, and less than 1% of cells had larger fibrillar inclusion bodies. However, during the 4th day, formation of fibrillar inclusion increased greatly (Fig. 2*B*). To confirm the time courses for the different aggregate species, we have recently established a biochemical method by which small non-fibrillar aggregates and fibrillar inclusions can be separated by their sizes and quantitated. After a series of extraction steps using detergent and basic pH, small non-fibrillar aggregates and fibrillar inclusions are separated into the supernatant and pellet, respectively, by a centrifugation at 80 × *g* (43). When this procedure was applied to the time-course study, we found that small aggregates in the supernatant appeared at day 3 and sustained until day 4, whereas the inclusions in the pellet became apparent no sooner than day 4 (Fig. 2*C*), confirming that small non-fibrillar aggregates appear before the formation of fibrillar inclusions. Given the dye-binding property and the kinetic behavior, we propose that the

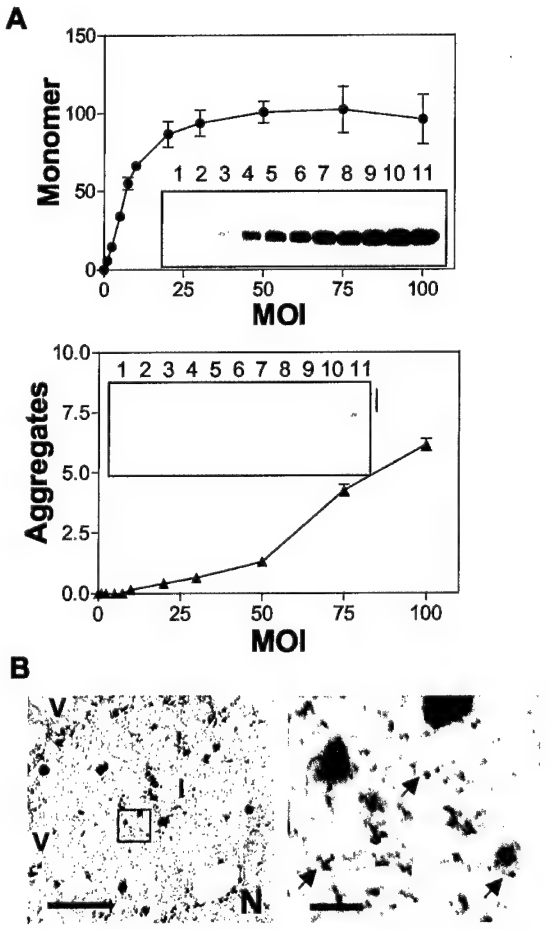

FIG. 1. **Non-linear relationship between the production of monomeric α-synuclein and its aggregation.** *A*, COS-7 cells were infected with different amount of adenoviral vector (adeno/α-syn) carrying α-synuclein cDNA and incubated for 3 days, and the levels of monomers and aggregates were measured from detergent-soluble and insoluble fractions, respectively. Empty viral vector was added so as to make the total number of viral particles in each sample constant. Arbitrary optical density units are plotted in the *graphs*. *Insets* are the representative autoradiograms of the Western blotting using LB509 antibody and ^{125}I-labeled secondary antibody. Specific m.o.i. values used in the Western analysis are: *lane 1*, 0; *lane 2*, 1; *lane 3*, 2.4; *lane 4*, 5; *lane 5*, 7.4; *lane 6*, 10; *lane 7*, 20; *lane 8*, 30; *lane 9*, 50; *lane 10*, 75; and *lane 11*, 100. The *vertical line* on the *right side* of the *inset* indicates the stacking gel portion. *B*, juxtanuclear inclusion contains fibrils that are labeled with LB509 antibody. The *image* on the *right side* is the high magnification view of the *boxed region* in the *left image*. *Arrows* indicate immunogold particles. No immunogold labeling was found in α-synuclein non-expressers. *Scale bars*, 1 μm (*left image*) and 0.1 μm (*right image*). *N*, nucleus; *V*, vacuole; *I*, juxtanuclear inclusion body.

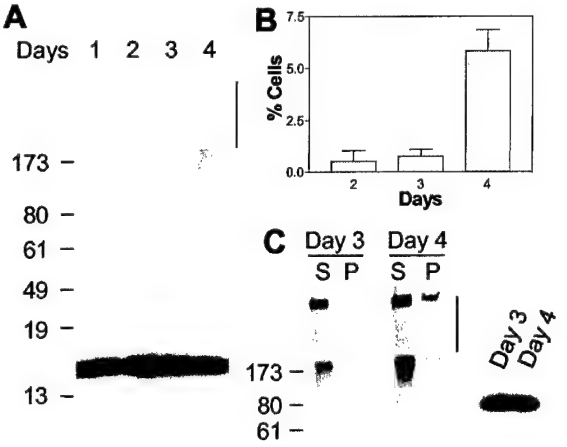

FIG. 2. **Appearance of small non-fibrillar aggregates precedes the formation of fibrillar inclusions in cells.** *A*, time-dependent changes in the levels of monomers and aggregates at the m.o.i. of 75 were measured from detergent-soluble (*lower panel*) and insoluble (*upper panel*) fractions, respectively. The *vertical line* on the *right side* indicates the stacking gel portion. *B*, the percentages of cells that contain juxtanuclear inclusion bodies were calculated at the indicated time points. α-Synuclein was expressed at m.o.i. of 75. Images were obtained from two optical sections to ensure the detection of inclusion bodies that are located in a different plane. *C*, fibrillar inclusions (*lane P*) and prefibrillar aggregates (*lane S*) were separated based on their sizes at days 3 and 4 and analyzed by Western blotting. The *left* and *right panels* show the detergent-insoluble aggregates and soluble monomers, respectively. The *vertical line* indicates the stacking gel portion.

small punctate aggregates are the cytoplasmic equivalents of prefibrillar intermediates of fibrillation.

Golgi Fragmentation by Prefibrillar α-Synuclein Aggregates—To investigate cellular consequences specific to α-synuclein aggregation, we have examined the morphology of Golgi apparatus (GA) for two reasons: (i) α-synuclein aggregates may target membranous organelles, because aggregates in our cell system appear initially in the membrane fraction,[2] consistent with the earlier finding in cell-free assay that membrane-bound α-synuclein forms aggregates more efficiently than the cytosolic α-synuclein (15), (ii) fragmentation of GA has been found in several neurodegenerative diseases, including Alzheimer's disease (AD), amyotrophic lateral sclerosis (ALS), Creutzfeldt-Jakob disease (CJD), and multiple system atrophy (MSA) (16–18). Especially, the pathology of MSA is characterized by α-synuclein-positive inclusion bodies of neurons and oligodendrocytes (19–21). Thus, the morphological integrity of GA was analyzed with respect to the α-synuclein aggregation states using an immunofluorescence microscopy with the antibody against a cis-Golgi-specific matrix protein GM130. In cells with diffuse α-synuclein staining, the GA has normal compact morphology near the nucleus (Fig. 3*A*). However, the cells with prefibrillar aggregates frequently show fragmentation and dispersion of the GA (Fig. 3, *B* and *C*). To determine if Golgi fragmentation is an aggregation-induced event, cells with fragmented Golgi were counted at different m.o.i. (Fig. 3*D*). Despite the presence of a high level of soluble α-synuclein, Golgi fragmentation at a m.o.i. of 20 was not different from the basal level. On the other hand, the Golgi fragmentation was significantly increased when prefibrillar aggregates formed with stable monomer levels (m.o.i. 75) (Fig. 3*D*), suggesting that increase of α-synuclein aggregates, rather than the monomer, might be the cause of Golgi fragmentation. To confirm the correlation between α-synuclein aggregation and Golgi fragmentation, an independent experiment was carried out to score the Golgi fragmentation in a population of cells that contained small punctate aggregates. Golgi fragmentation was found far more frequently in the population with the aggregates (88.9% at m.o.i. 75 and 66.7% at m.o.i. 20) than in the general population (11.5% at m.o.i. 75 and 4.3% at m.o.i. 20) (Fig. 3*E*). In contrast, expression of green fluorescent protein to ~9.1% of total cellular protein did not cause dramatic changes in the Golgi morphology (data not shown), suggesting that Golgi fragmentation is not a general consequence of overproduction of soluble proteins.

To determine the effects of α-synuclein aggregates on other Golgi compartments, we examine the morphologies of trans- and mid-Golgi using antibodies against TGN46, an integral component of trans-Golgi membrane, and mannosidase II, a mid-Golgi resident enzyme. Dual immunofluorescence staining shows that the aggregate-induced Golgi fragments contain

[2] J. S. Lee and S.-J. Lee, unpublished data.

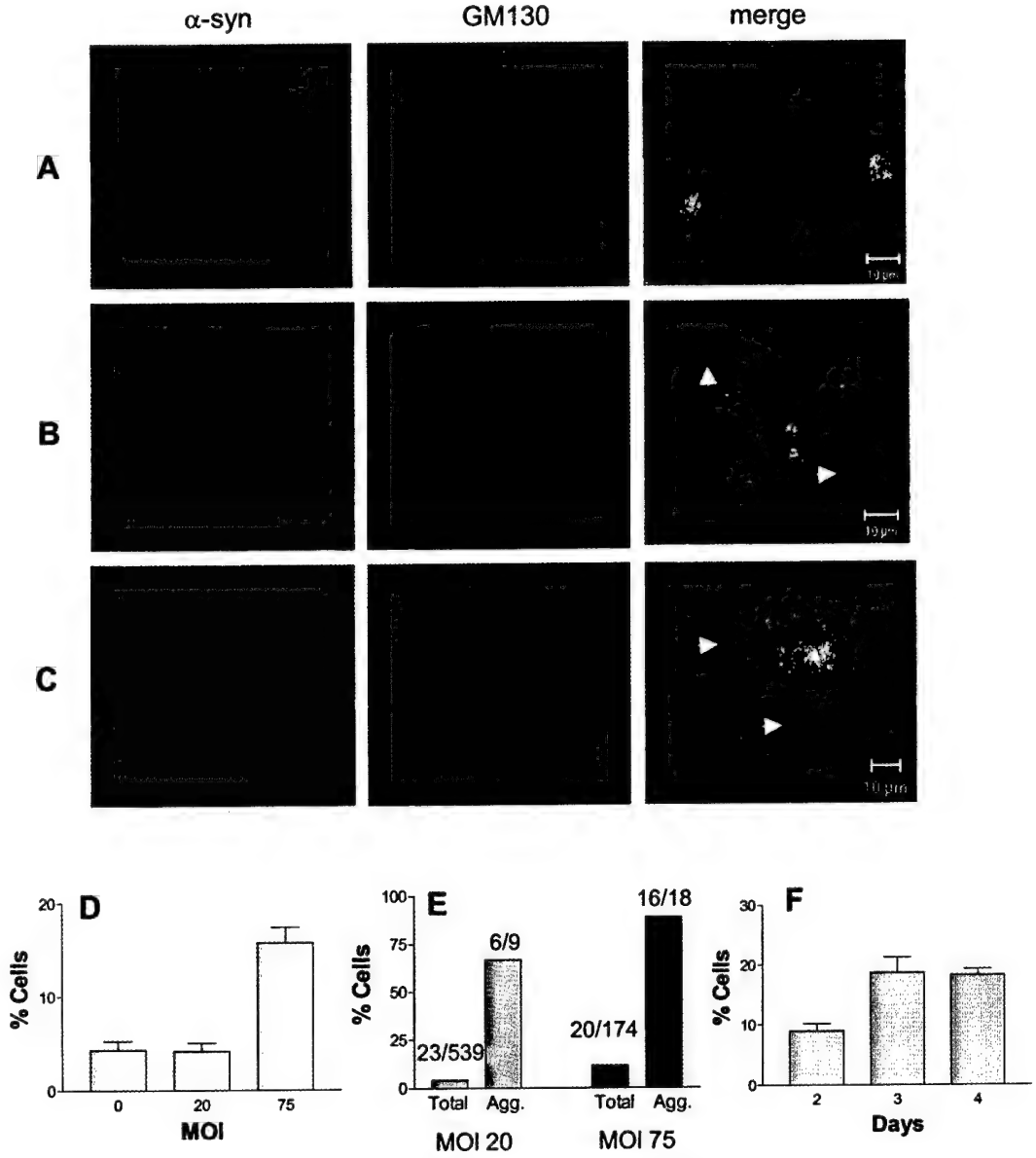

FIG. 3. **Occurrence of small α-synuclein aggregates is tightly associated with Golgi fragmentation.** Golgi morphology was visualized using an antibody against GM130. α-Synuclein was expressed at the m.o.i. of 75, and α-synuclein aggregation (*red*) and Golgi morphology (*green*) were analyzed at day 3. Nuclei were stained with Hoechst 33258 (*blue*). *A*, diffuse α-synuclein staining and normal Golgi morphology. *B* and *C*, prefibrillar aggregates (*arrowheads*) that are dispersed throughout the cytoplasm and fragmented Golgi. Aggregates shown in *C* are larger than the ones in *B*. Both types are non-fibrillar and associated with the Golgi fragmentation. *D*, percentage of cells with fragmented Golgi. α-Synuclein was expressed at given m.o.i. values, and the cells were labeled with the antibodies against α-synuclein (7071 (5)) and GM130 at day 3. The total number of viral particles was adjusted to be equivalent by adding an appropriate amount of empty viral vector to each sample. *E*, in a separate experiment, the number of cells with Golgi fragmentation was counted in a total cell population (*total*) and in a group of cells with prefibrillar α-synuclein aggregates (*Agg.*) at day 3. *Numbers* above the *bars* represent the number of cells with fragmented Golgi per the number of cells counted. *F*, time course of the Golgi fragmentation was analyzed at the m.o.i. of 75 as described in *D*. *Scale bars*, 10 μm.

both GM130 and TGN46. Furthermore, these proteins stayed segregated to the opposite poles in these fragments as in the normal compact GA (Fig. 4*A*), indicating that the cis-trans polarity was maintained even after the fragmentation. When the Golgi fragments were co-stained for GM130 and mannosidase II, the segregation of these proteins was also evident within the single fragments (Fig. 4*B*). However, the segregation was not as obvious as the co-staining of GM130 and TGN46, probably due to their relative distance between the compartments. These results suggest that α-synuclein aggregate-induced Golgi fragmentation occurs in the entire Golgi complex without obvious disturbance of the cis-trans polarity.

Reduction in Cell Surface Level of Dopamine Transporter—While passing through the Golgi stacks, secretory and membrane proteins undergo a series of covalent modifications, such as glycosylation and deglycosylation, and the fully mature proteins are sorted to their final destinations. To assess the functional consequence of the aggregate-induced Golgi fragmentation, we measured the changes in the cell surface level of a plasma membrane protein dopamine transporter (DAT). The cells were infected with different amounts of adeno/α-syn and then transfected with DAT expression plasmids on the following day. After 2 more days of incubation, the cell surface proteins were covalently labeled with biotin and separated from the cytoplasmic proteins (non-biotinylated) using streptavidin resin. Western analysis of these fractions shows that cell surface level of DAT was reduced in the prefibrillar aggregate-producing condition (m.o.i. 75), compared with the empty vector alone (m.o.i. 0) (Fig. 5). However, increase of monomeric α-synuclein level did not result in any change in the cell surface

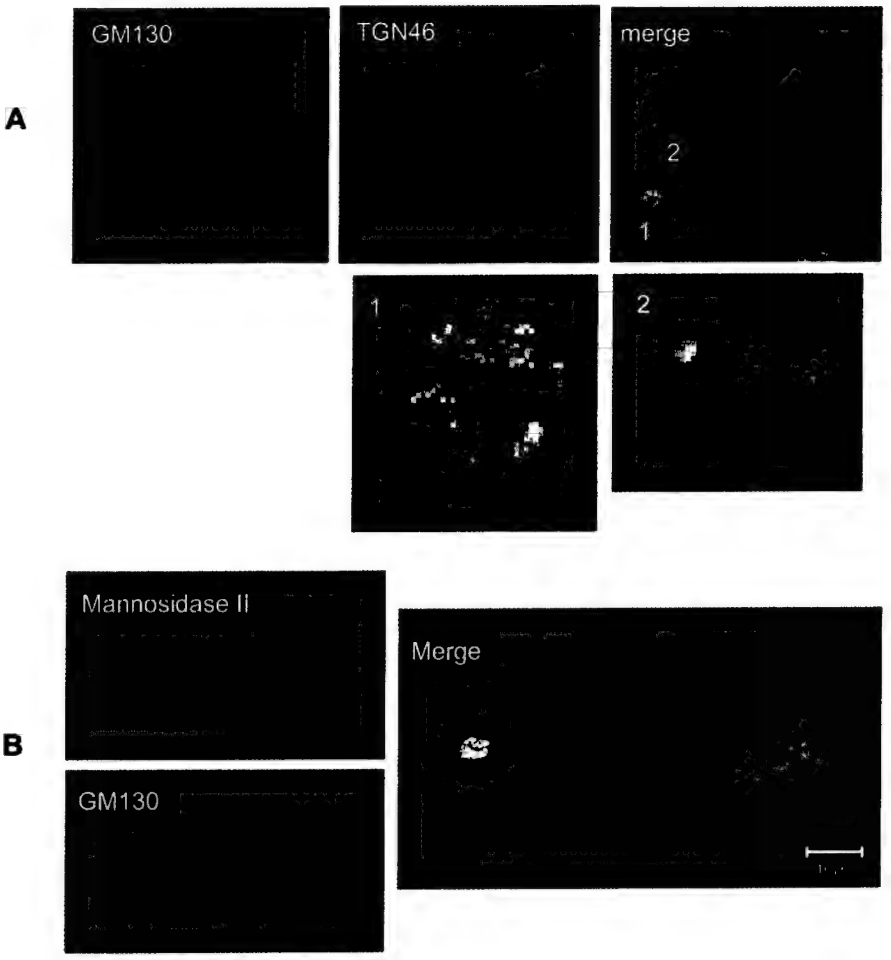

FIG. 4. **α-Synuclein aggregates induce the Golgi fragmentation in the entire Golgi complex.** Aggregates were induced as in Fig. 3, and the cis- and trans-Golgi (*A*) or cis- and mid-compartments (*B*) were stained with the antibodies against GM130 (*red*) and TGN46 (*green*) (*A*), or GM130 (*green*) and mannosidase II (*red*) (*B*), respectively. The *lower images* in *A* are the high magnification views of normal (*1*) and fragmented Golgi (*2*). Note that the Golgi fragments contain all the markers that represent individual cisternae and still maintain the cis-trans polarity. *Scale bars*, 10 μm.

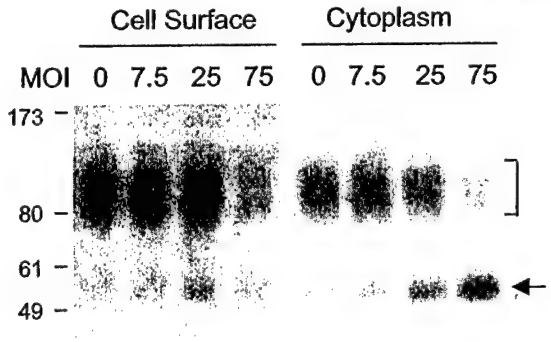

FIG. 5. **Reduction in cell surface expression of DAT and accumulation of biosynthetic intermediates in cytoplasm.** After the expression of α-synuclein at different m.o.i. values for 3 days, cell surface levels of DAT were measured as described under "Materials and Methods." Note that the cell surface level of DAT was reduced only in the condition that makes α-synuclein aggregates. Also note that α-synuclein monomer levels are similar at m.o.i. values 25 and 75 (see Fig. 1). The *bracket* and the *arrow* indicate mature DAT and endoH-sensitive intermediate, respectively. Reduction in cell surface DAT is associated with the accumulation of biosynthetic intermediates in cytoplasm. Total amounts of viral particles were normalized with empty vector.

expression of DAT (Fig. 5, see m.o.i. 7.5 and 25). Reduction in cell surface DAT was accompanied by the molecular mass shift of cytoplasmic DAT from 90–100 kDa to 56 kDa (Fig. 5). The former corresponds to the endoglycosidase H (endoH)-resistant mature protein, and the latter is the endoH-sensitive biosynthetic intermediate (14). Because the endoH resistance is obtained in mid-Golgi compartment, these data imply that the newly synthesized proteins cannot reach the mid-Golgi in an aggregate-producing condition. In contrast, accumulation of the endoH-sensitive form indicates that the overall protein synthesis, and the initial glycosylation may not be compromised in this condition. These results suggest that prefibrillar α-synuclein aggregates cause the impaired protein trafficking and maturation through the biosynthetic pathway, probably by disrupting Golgi transport.

Consistent with the finding that the biosynthesis of endoH-sensitive form of DAT is not affected by α-synuclein aggregation, the gross morphology and distribution of endoplasmic reticulum (ER) seem to remain unchanged in the presence of α-synuclein aggregates. Normally, the ER shows a dispersed reticular pattern throughout the cytoplasm. This pattern was maintained regardless of the α-synuclein aggregation state or structural integrity of GA in the cytoplasm (Fig. 6), suggesting that the α-synuclein aggregates have little effect on the ER morphology.

Inclusion Bodies May be the Response of the Cell to the Toxic Protein Aggregates—In contrast to the prefibrillar aggregates, no clear association was found between the fibrillar inclusions and the Golgi fragmentation. First, an increase in Golgi fragmentation occurs before the appearance of fibrillar inclusions (Figs. 2*B* and 3*F*). Second, the size of the cell population that contains fragmented GA does not increase during the fourth day when a sudden increase in the number of fibrillar inclusions takes place (Figs. 2*B* and 3*F*). Finally, fragmented GA was rarely observed in the cells with fibrillar inclusions. Instead, two types of GA morphology were associated with fibrillar inclusions: in most cases, Golgi components were confined and dispersed inside the fibrillar inclusions (Fig. 7*A*), and occasionally, some cells maintained the compact, although

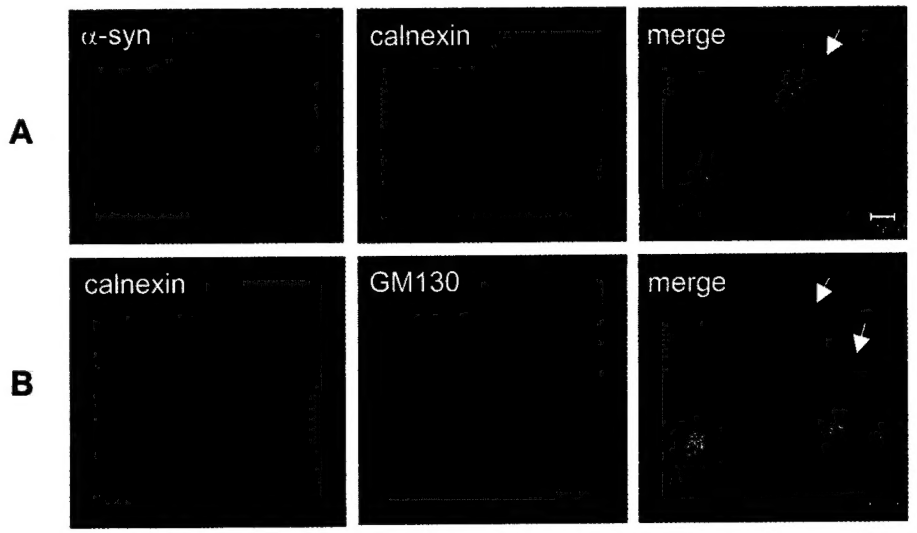

FIG. 6. **No gross changes in ER morphology and distribution.** α-Synuclein was expressed at m.o.i. 75 for 3 days. *A*, co-staining of α-synuclein (*red*) and ER (*green*). ER was stained with anti-calnexin antibody. A cell with aggregates is indicated with an *arrow*. No changes in ER morphology can be recognized in the presence of aggregates, compared with the cells with diffuse α-synuclein staining. *B*, co-staining of calnexin (*red*) and GM130 (*green*). The cells with fragmented GA are marked with *arrows*. ER morphology and distribution seem unchanged regardless of the state of GA. *Scale bars*, 10 μm

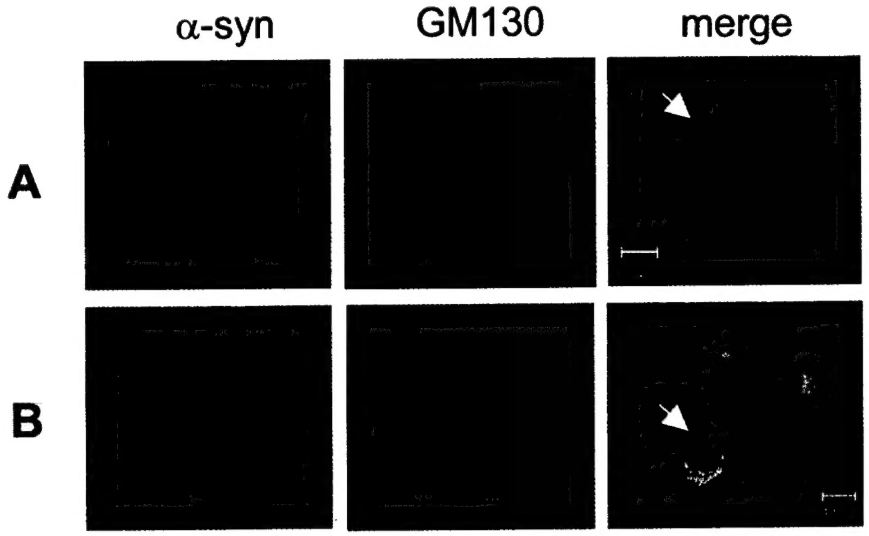

FIG. 7. **GA in the cells with inclusion bodies.** α-Synuclein was expressed at m.o.i. 75 for 4 days. *A*, a fibrillar inclusion (*arrow*) containing GM130 (*green*). GM130 is dispersed within the inclusion body. The inclusion body shown here is present on a different optical plane from the majority of other cellular components. This type of inclusion is much more frequently found than the type shown in *B*. *B*, distorted GA adjacent to a fibrillar inclusion (*arrow*). *Scale bars*, 10 μm.

slightly distorted, morphology of GA that surrounded the juxtanuclear fibrillar inclusions (Fig. 7*B*). The distorted compact Golgi that is adjacent to inclusion has also been reported previously in a study using a GFP-250 (N-terminal 252 amino acids of p115) chimera protein (22). These two types of Golgi morphology might be explained by the difference in the rate of conversion of prefibrillar intermediates to fibrillar inclusions; fast sequestration of the prefibrillar aggregates into the inclusions before they damage the GA might lead to the distorted compact Golgi adjacent to the inclusion body. Alternatively, inclusions could be formed from two different prefibrillar species, only one of which is capable of Golgi fragmentation. In any case, the facts that Golgi fragmentation occurs before the formation of inclusions and that some cells maintain the compact Golgi structure despite the presence of inclusions suggest that the inclusions themselves may not be the direct cause of the morphological disruption of the GA. Rather, co-staining of the fibrillar inclusions with α-synuclein and Golgi marker suggests that the inclusions might be a consequence of an attempt by the cell to remove abnormal protein aggregates and impaired organelles from the cytoplasm.

Consistent with this interpretation, intact lysosomes and mitochondria accumulated in the juxtanuclear region at what appears to be an early stage of inclusion formation (Fig. 8, *A* and *C*) and are also present in the compact inclusions (Fig. 8, *B* and *D*). Lysosomes and mitochondria, which normally tend to be dispersed in the cytoplasm, showed a rather localized pattern in the juxtanuclear region in the presence of the prefibrillar α-synuclein aggregates (Fig. 8, *A* and *C*). These organelles showed no sign of fragmentation and appear to be functionally intact, because the fluorescent dyes used in this study selectively accumulate in cellular compartment with low internal pH (Lysotracker) or with the membrane potential (Mitotracker). EM study also showed the accumulation of fragmented Golgi (Fig. 9, *box 1*) and intact mitochondria in the juxtanuclear region (Fig. 9). In addition, autophagosomes and lysosomes can be found in this area at the early stage of inclusion formation (Fig. 9, *box 2*). Proteasomes and chaperone molecules were also accumulated near the nucleus in the cells with α-synuclein aggregates (43). It has been suggested that the juxtanuclear pericentriolar region serves as the main location in which both the autophagic/lysosomal system and ubiquitin-proteasome system execute their degradation function to remove abnormal proteins and damaged organelles (23–25). Thus, the localization of functional lysosomes and mitochondria in the juxtanuclear region may be the manifestation of defense mechanisms of the cell against the protein aggregates. Together, these results suggest that the formation of α-synuclein aggregates triggers the action of the cellular defense system, which is represented by the accumulation of these aggregates and impaired organelles in the juxtanuclear

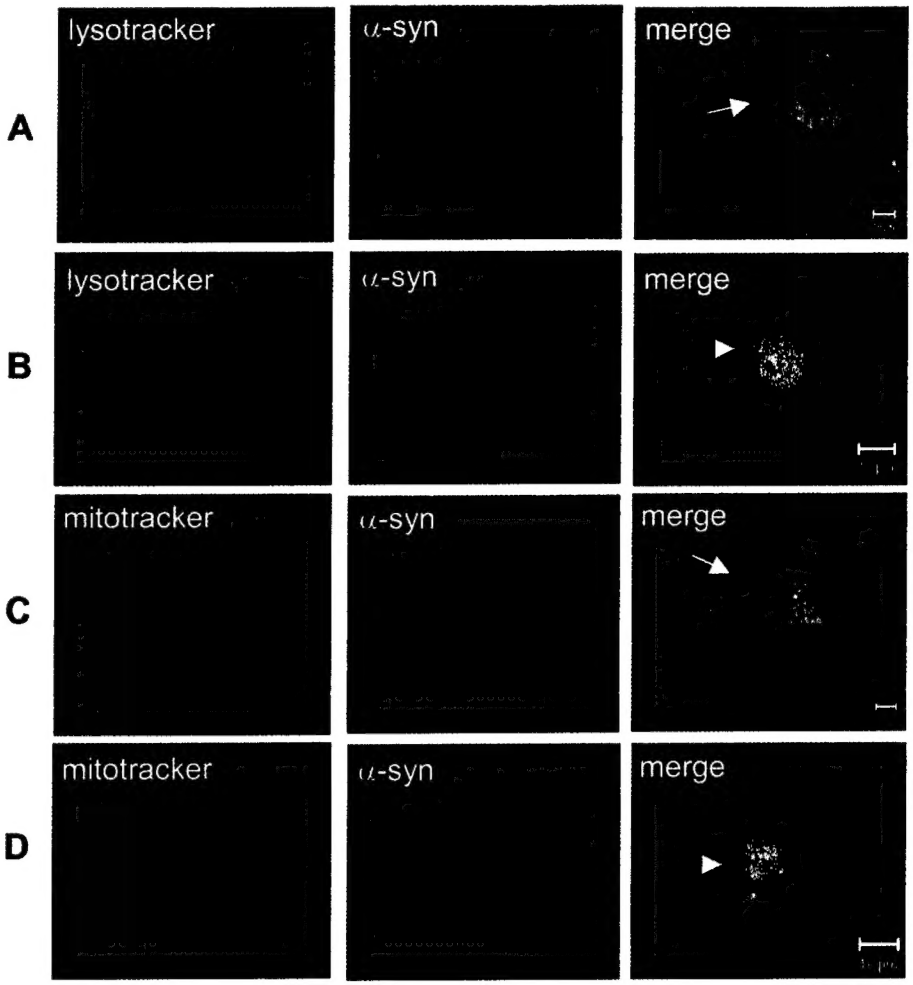

FIG. 8. **Accumulation of lysosomes and mitochondria at the inclusion-forming site in aggregate-containing cells.** α-Synuclein was expressed at m.o.i. 75 for 4 days. Cells with prefibrillar aggregates are indicated with *arrows*. *A*, lysosomes with internally low pH were labeled with Lysotracker. Lysosomes and α-synuclein aggregates were found in the juxtanuclear area that appears to be a "pre-inclusion" state. *B*, Lysotracker also stains the juxtanuclear inclusion body (*arrowhead*). *C*, mitochondria with intact membrane potential were labeled with Mitotracker. Functional mitochondria and α-synuclein were accumulated in the juxtanuclear region. *D*, mitochondria are also accumulated within the inclusion body (*arrowhead*). *Scale bars*, 10 μm.

region along with the mitochondria, autophagosomes/lysosomes, and proteasomes.

Cytotoxicity of Prefibrillar α-Synuclein Aggregates—A cytotoxic effect of α-synuclein has been reported in several mammalian cell systems (26–29). However, the nature of toxic species has not been determined. To assess the cytotoxic effect of α-synuclein aggregates, we measured cell viability as a function of the occurrence of the aggregates. An increase of monomer, without forming aggregates, did not affect the viability (m.o.i. 0–20) (Figs. 1*A* and Fig. 10*A*, day 3). In contrast, cell viability was significantly reduced when aggregates formed without increasing the monomer level (Fig. 10, *A* and *B*, day 3). Tight correlation between reduction in cell viability and α-synuclein aggregation was also found in the time-course study. Aggregates were formed at slower rates at lower m.o.i. values (m.o.i. 20 and 50), and when they became apparent on the fourth day, the viability was reduced correspondingly (Fig. 10, *A* and *B*). Like the Golgi fragmentation, reduction in cell viability occurred before the appearance of the fibrillar inclusions (Fig. 10*A*, day 3 at the m.o.i. of 70, and see also Fig. 2, *B* and *C*), implicating that the cytotoxic effect might be conferred by the prefibrillar aggregates. These results suggest that the cytotoxic effect of α-synuclein depends on its ability to form aggregates, especially the prefibrillar intermediates.

DISCUSSION

In this study, we report two biological effects of cytoplasmic α-synuclein aggregates; fragmentation of the GA and cell death. The fact that these effects correlate only with the formation of aggregates, and not with the monomer level, suggests that occurrence of these effects depends on the formation of higher order, quaternary structures. The prefibrillar intermediates seem to be responsible for these effects, because both of the effects occur in the presence of small prefibrillar aggregates, and before the formation of fibrillar inclusions. We were able to distinguish specific effects of prefibrillar intermediates from those of monomers and fibrillar inclusions by taking advantage of the following features of our experimental system. First, once the monomer level reaches a plateau, only aggregates increase in response to an increasing amount of α-synuclein cDNA without changing the monomer level. This phenomenon provides an effective means to distinguish the effects of aggregates from those of monomers. Second, the ability to define naturally occurring prefibrillar aggregates and fibrillar inclusions biochemically, allowed kinetic analysis of each species. This study showed that the aggregation process of α-synuclein in cells, similar to the findings in test tube, involves prefibrillar intermediates in the course of forming fibrillar inclusions (43). More importantly, such a kinetic delay of the inclusion formation enabled us to distinguish the cytophysiological effects of prefibrillar intermediates and fibrillar inclusions.

Earlier examinations of human brain tissues and animal models have shown that the Golgi fragmentation was associated with the neurodegenerative phenotypes. Fragmentation of the GA has been found in human neurodegenerative diseases, including AD, ALS, CJD, and MSA (16–18). Moreover, transgenic mice expressing ALS-linked mutant superoxide dismutase 1 showed Golgi fragmentation in spinal cord motor

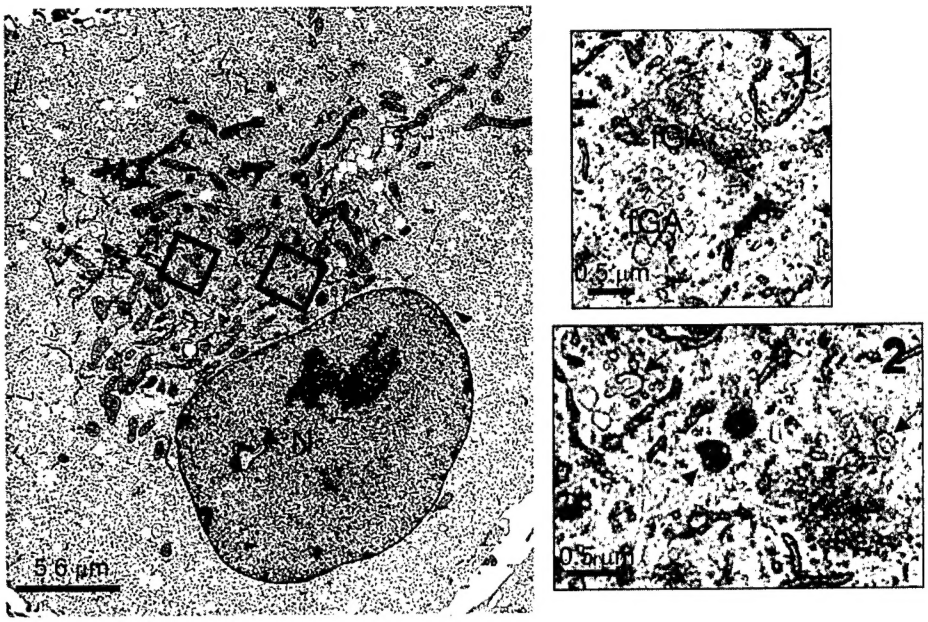

FIG. 9. **EM analysis of the pre-inclusion state.** The cells were infected with adeno/α-syn at m.o.i. 75, incubated for 4 days, and processed for EM as described under "Materials and Methods." Most inclusions have compact structure with clear boundary. Occasionally, we observe what appears to be an early stage of inclusion formation. In this pre-inclusion stage, mitochondria (*M*), autophagosome precursors (*arrows*, *box 2*), lysosomes (*arrowhead*, *box 2*), and fragmented GA (*fGA*, *box 1*) are accumulated in the juxtanuclear region, and hardly detected outside this region. Neither the pre-inclusion stage nor the compact inclusion body could be found in the cells that were infected with empty viral vector. *Scale bars*, 5.6 μm for the *main image* and 0.5 μm for the *box images*.

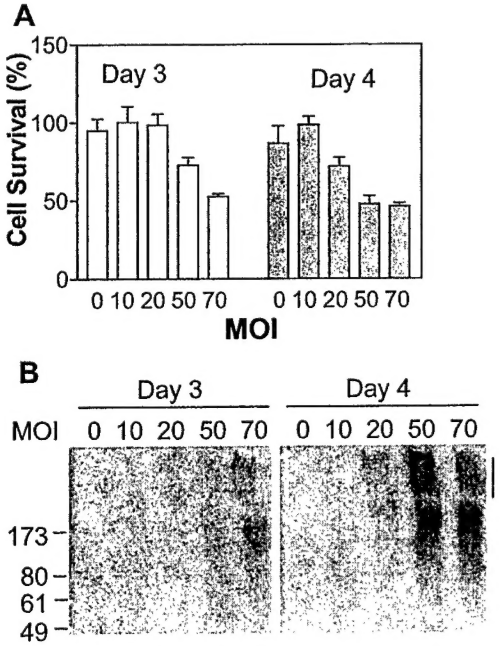

FIG. 10. **Cytotoxic effect of α-synuclein is dependent on the aggregation and occurs before the formation of fibrillar inclusions.** *A* and *B*, COS-7 cells were infected with adeno/α-syn at given m.o.i. values (the total number of viral particles was normalized by adding an appropriate amount of empty vector), and each sample was subjected to the trypan blue exclusion assay (*A*) and Western blotting with LB509 (*B*). The percentage of live cell number was calculated, with the non-expressor at day 3 as being 100%. The Western blotting was performed with the detergent-insoluble fractions.

neurons in an early, preclinical stage, implicating the role of Golgi fragmentation in the early stage of neurodegeneration (30). Our present study links this well-documented pathological feature of neurodegenerative diseases, the Golgi fragmentation, to the prefibrillar aggregate form of α-synuclein. Although our results imply the correlation between Golgi fragmentation and cell death, they are not sufficient to suggest the cause/effect relationship between these two. Nevertheless, given the importance of the GA in maturation and trafficking of essential proteins and lipids, we speculate that synaptic sites might be particularly vulnerable to Golgi dysfunction. It is, therefore, noteworthy that transgenic mice producing non-fibrillar α-synuclein aggregates in neurons suffer from presynaptic degeneration in nigrostriatal system (31).

Whether inclusion bodies are toxic entities or harmless by-products or even a part of a protective mechanism has been one of the central issues in amyloid-associated disorders. Our present study shows that (i) Golgi fragmentation and cell death are observed before the formation of inclusion bodies in mixed cell populations and that (ii) α-synuclein aggregates are pulled into the "pre-inclusion" area in the juxtanuclear region along with cellular defense organelles, such as autophagic/lysosomal vesicles and mitochondria. These results are consistent with the notion that inclusion bodies *per se* might not be directly harmful to cells, rather, they are consequences of the efforts to remove abnormal protein aggregates and damaged organelles from the cytoplasm. In a recent study using a *Drosophila* model in which exogenous expression of human α-synuclein induced Lewy body-like inclusions and dopaminergic neuronal loss, overproduction of a molecular chaperone hsp70 alleviated the neurodegenerative phenotype without reducing the number of inclusion bodies (8). This study also argues against the direct role of α-synuclein-positive inclusion body in the degenerative process. The non-causal relationship of inclusion bodies and cell death has also been proposed in other protein aggregation systems. A degenerative phenotype and the formation of detectable inclusion bodies have been dissociated in cell and animal models that overexpress expanded polyglutamine-containing proteins (32–36). In another study using a transgenic mouse model that expresses familial ALS-associated mutant superoxide dismutase 1, small detergent-insoluble protein complex occurs before the onset of disease phenotype, whereas the inclusion bodies can be detected once the clinical symptom is evident (37). Therefore, regardless of the constituent protein, the presence of inclusion bodies itself does not seem to be directly responsible for the cell death. However, these results do not exclude the possibility that the "process" of inclusion body formation might damage the cells; here, we refer to the process as the cellular events related to the inclusion formation *after* the diffusion-limited peripheral aggregation. For example, sequestration and depletion of vital proteins and organelles, such as proteasomes, mitochondria, and lysosomes, from the cytoplasm, as seen in the early stage of α-synuclein inclusion formation, could make the cells vulnerable to any secondary stresses. The sequestration, thus the reduced cellular activity, of the ubiquitin-proteasome system has indeed

been proposed to be a general consequence of protein aggregation that can lead to cell death (38).

Interfering with the microtubule-mediated transport could also lead to the Golgi fragmentation. For example, microtubule-disrupting agents, such as nocodazole, cause a redistribution of Golgi proteins to ER exit sites (39). Thus, the Golgi fragmentation observed in our study could be a secondary consequence of overloading the microtubule-dependent transport system with the aggregates or of halting the trafficking at the negative ends of microtubules due to the accumulation of α-synuclein aggregates, rather than the direct effect of the α-synuclein aggregates. We do not have conclusive evidence to support either of these possibilities, but the architecture of the fragmented Golgi indicates that more complex mechanism may underlie the α-synuclein aggregate-induced Golgi fragmentation than the interference of microtubule-dependent transport. In case of the aggregate-induced Golgi fragmentation, components of different Golgi compartments seem to stay together in the Golgi fragments with the intact cis-trans polarity. This finding disagrees with what was observed during the nocodazole-induced Golgi fragmentation, in which trans-Golgi proteins were scattered more rapidly than mid-Golgi proteins, suggesting the separation of Golgi subcompartments from each other prior to the scattering (40).

Unlike the small punctate aggregates, juxtanuclear inclusion bodies contain α-synuclein fibrils. No evidence has been obtained for the presence of fibrillar α-synuclein aggregates outside the juxtanuclear inclusions. These findings implicate that, although the mechanism is not understood at present, the structural transition of prefibrillar intermediates into thermodynamically more stable fibrils occurs after they are transported and deposited in the inclusion-forming site (43). A recent study showed that α-synuclein fibrils were far less efficient in disrupting bilayer membranes than protofibrils (41), suggesting an inert nature of fibrils. In other studies using recombinant proteins or synthetic peptides that are not implicated in any disease, fibrils were non-toxic when treated to cultured cells, whereas the same treatment with non-fibrillar aggregates, which precede formation of fibrils, resulted in cell death (42). Therefore, formation of fibrillar inclusion bodies might protect the cells from the cytotoxicity of aggregates, not only by removing the prefibrillar aggregates from the cytoplasm but also by providing the right environment for converting them to inert fibrils.

In conclusion, the results presented in this report suggest that the pathogenic property of α-synuclein may not stem from its primary structure but from its ability to form toxic aggregates, particularly the prefibrillar aggregates. Importantly, fibrillar inclusions may not be directly toxic, rather, they may represent the outcome of the natural way the cell handles abnormal protein aggregates that are formed randomly throughout the cytoplasm. Thus, both preventing the formation of aggregates and accelerating the conversion of prefibrillar intermediates to fibrillar inclusions might be logical strategies for intervening the pathogenic progress of LB diseases.

Acknowledgments—We thank D. Di Monte and A. Manning-Bog for helpful comments on the manuscript. We also thank P. T. Lansbury for 7071 antibody, H. Melikian for DAT expression plasmid, and N. Ghori for the technical assistance for the EM.

REFERENCES

1. Hardy, J., and Gwinn-Hardy, K. (1998) *Science* **282,** 1075–1079
2. Trojanowski, J. Q., Goedert, M., Iwatsubo, T., and Lee, V. M.-Y. (1998) *Cell Death Differ.* **5,** 832–837
3. Goedert, M. (2001) *Nat. Rev. Neurosci.* **2,** 492–501
4. Giasson, B. I., Uryu, K., Trojanowski, J. Q., and Lee, V. M.-Y. (1999) *J. Biol. Chem.* **274,** 7619–7622
5. Conway, K. A., Harper, J. D., and Lansbury, P. T., Jr. (2000) *Biochemistry* **39,** 2552–2563
6. Serpell, L. C., Berriman, J., Jakes, R., Goedert, M., and Crowther, R. A. (2000) *Proc. Natl. Acad. Sci. U. S. A.* **97,** 4897–4902
7. Giasson, B. I., Duda, J. E., Quinn, S. M., Zhang, B., Trojanowski, J. Q., and Lee, V. M.-Y. (2002) *Neuron* **34,** 521–533
8. Auluck, P. K., Chan, H. Y., Trojanowski, J. Q., Lee, V. M.-Y., and Bonini, N. M. (2002) *Science* **295,** 865–868
9. Conway, K. A., Lee, S.-J., Rochet, J. C., Ding, T. T., Williamson, R. E., and Lansbury, P. T., Jr. (2000) *Proc. Natl. Acad. Sci. U. S. A.* **97,** 571–576
10. Conway, K. A., Rochet, J. C., Bieganski, R. M., and Lansbury, P. T., Jr. (2001) *Science* **294,** 1346–1349
11. Lee, H.-J., Shin, S. Y., Choi, C., Lee, Y. H., and Lee, S.-J. (2002) *J. Biol. Chem.* **277,** 5411–5417
12. Lee, S.-J., Liyanage, U., Bickel, P. E., Xia, W., Lansbury, P. T., Jr., and Kosik, K. S. (1998) *Nat. Med.* **4,** 730–734
13. Bouley, D. M., Ghori, N., Mercer, K. L., Falkow, S., and Ramakrishnan, L. (2001) *Infect. Immun.* **69,** 7820–7831
14. Melikian, H. E., and Buckley, K. M. (1999) *J. Neurosci.* **19,** 7699–7710
15. Lee, H.-J., Choi, C., and Lee, S.-J. (2002) *J. Biol. Chem.* **277,** 671–678
16. Gonatas, N. K., Gonatas, J. O., and Stieber, A. (1998) *Histochem. Cell Biol.* **109,** 591–600
17. Sakurai, A., Okamoto, K., Fujita, Y., Nakazato, Y., Wakabayashi, K., Takahashi, H., and Gonatas, N. K. (2000) *Acta Neuropathol.* **100,** 270–274
18. Sakurai, A., Okamoto, K., Yaguchi, M., Fujita, Y., Mizuno, Y., Nakazato, Y., and Gonatas, N. K. (2002) *Acta Neuropathol.* **103,** 550–554
19. Wakabayashi, K., Hayashi, S., Kakita, A., Yamada, M., Toyoshima, Y., Yoshimoto, M., and Takahashi, H. (1998) *Acta Neuropathol.* **96,** 445–452
20. Spillantini, M. G., Crowther, R. A., Jakes, R., Cairns, N. J., Lantos, P. L., and Goedert, M. (1998) *Neurosci. Lett.* **251,** 205–208
21. Dickson, D. W., Liu, W., Hardy, J., Farrer, M., Mehta, N., Uitti, R., Mark, M., Zimmerman, T., Golbe, L., Sage, J., Sima, A., D'Amato, C., Albin, R., Gilman, S., and Yen, S. H. (1999) *Am. J. Pathol.* **155,** 1241–1251
22. Garcia-Mata, R., Bebok, Z., Sorscher, E. J., and Sztul, E. S. (1999) *J. Cell Biol.* **146,** 1239–1254
23. Garcia-Mata, R., Gao, Y. S., and Sztul, E. (2002) *Traffic* **3,** 388–396
24. Kopito, R. R. (2000) *Trends Cell Biol.* **10,** 524–530
25. Wigley, W. C., Fabunmi, R. P., Lee, M. G., Marino, C. R., Muallem, S., DeMartino, G. N., and Thomas, P. J. (1999) *J. Cell Biol.* **145,** 481–490
26. Ostrerova, N., Petrucelli, L., Farrer, M., Mehta, N., Choi, P., Hardy, J., and Wolozin, B. (1999) *J. Neurosci.* **19,** 5782–5791
27. Zhou, W., Schaack, J., Zawada, W. M., and Freed, C. R. (2002) *Brain Res.* **926,** 42–50
28. Iwata, A., Maruyama, M., Kanazawa, I., and Nukina, N. (2001) *J. Biol. Chem.* **276,** 45320–45329
29. Saha, A. R., Ninkina, N. N., Hanger, D. P., Anderton, B. H., Davies, A. M., and Buchman, V. L. (2000) *Eur. J. Neurosci.* **12,** 3073–3077
30. Mourelatos, Z., Gonatas, N. K., Stieber, A., Gurney, M. E., and Dal Canto, M. C. (1996) *Proc. Natl. Acad. Sci. U. S. A.* **93,** 5472–5477
31. Masliah, E., Rockenstein, E., Veinbergs, I., Mallory, M., Hashimoto, M., Takeda, A., Sagara, Y., Sisk, A., and Mucke, L. (2000) *Science* **287,** 1265–1269
32. Klement, I. A., Skinner, P. J., Kaytor, M. D., Yi, H., Hersch, S. M., Clark, H. B., Zoghbi, H. Y., and Orr, H. T. (1998) *Cell* **95,** 41–53
33. Saudou, F., Finkbeiner, S., Devys, D., and Greenberg, M. E. (1998) *Cell* **95,** 55–66
34. Cummings, C. J., Reinstein, E., Sun, Y., Antalffy, B., Jiang, Y., Ciechanover, A., Orr, H. T., Beaudet, A. L., and Zoghbi, H. Y. (1999) *Neuron* **24,** 879–892
35. Faber, P. W., Alter, J. R., MacDonald, M. E., and Hart, A. C. (1999) *Proc. Natl. Acad. Sci. U. S. A.* **96,** 179–184
36. Kazemi-Esfarjani, P., and Benzer, S. (2000) *Science* **287,** 1837–1840
37. Johnston, J. A., Dalton, M. J., Gurney, M. E., and Kopito, R. R. (2000) *Proc. Natl. Acad. Sci. U. S. A.* **97,** 12571–12576
38. Bence, N. F., Sampat, R. M., and Kopito, R. R. (2001) *Science* **292,** 1552–1555
39. Thyberg, J., and Moskalewski, S. (1999) *Exp. Cell Res.* **246,** 263–279
40. Yang, W., and Storrie, B. (1998) *Mol. Biol. Cell* **9,** 191–207
41. Volles, M. J., Lee, S.-J., Rochet, J. C., Shtilerman, M. D., Ding, T. T., Kessler, J. C., and Lansbury, P. T., Jr. (2001) *Biochemistry* **40,** 7812–7819
42. Bucciantini, M., Giannoni, E., Chiti, F., Baroni, F., Formigli, L., Zurdo, J., Taddei, N., Ramponi, G., Dobson, C. M., and Stefani, M. (2002) *Nature* **416,** 507–511
43. Lee H.-J., and Lee S.-J. (2002) *J. Biol. Chem.* **277,** 48976–48983